[24] P. Gastaminza, C. Whitten-Bauer, F.V. Chisari, Unbiased probing of the entire hepatitis C virus life cycle identifies clinical compounds that target multiple aspects of the infection, Proc. Natl. Acad. Sci. U. S. A. 107 (2010) 291–296.

[25] K. Chockalingam, R.L. Simeon, C.M. Rice, Z. Chen, A cell protection screen reveals potent inhibitors of multiple stages of the hepatitis C virus life cycle, Proc. Natl. Acad. Sci. U. S. A. 107 (2010) 3764–3769.

[26] P. de Medina, G. Favre, M. Poirot, Multiple targeting by the antitumor drug tamoxifen: a structure-activity study, Curr. Med. Chem. Anticancer Agents 4 (2004) 491–508.

[27] E.R. Prossnitz, J.B. Arterburn, L.A. Sklar, GPR30: a G protein-coupled receptor for estrogen, Mol. Cell. Endocrinol. 265–266 (2007) 138–142.

[28] P. Thomas, Y. Pang, E.J. Filardo, J. Dong, Identity of an estrogen membrane receptor coupled to a G protein in human breast cancer cells, Endocrinology 146 (2005) 624–632.

[29] M.K. Dennis, R. Burai, C. Ramesh, W.K. Petrie, S.N. Alcon, T.K. Nayak, C.G. Bologa, A. Leitao, E. Brailoiu, E. Deliu, N.J. Dun, L.A. Sklar, H.J. Hathaway, J.B. Arterburn, T.I. Oprea, E.R. Prossnitz, In vivo effects of a GPR30 antagonist, Nat. Chem. Biol. 5 (2009) 421–427.

*Send Orders of Reprints at reprints@benthamscience.org*

1616 *Current Drug Targets*, 2012, *13*, 1616-1621

# Long Non-Coding RNAs Involved in Cancer Development and Cell Fate Determination

Masatoshi Kitagawa[1,*], Yojiro Kotake[2] and Tatsuya Ohhata[1]

[1]*Department of Molecular Biology, Hamamatsu University School of Medicine, Hamamatsu, Japan;* [2]*Department of Biological and Environmental Chemistry, Faculty of Humanity-Oriented Science and Engineering, Kinki University, Osaka, Japan*

**Abstract:** The possible physiological significance of long non-coding RNAs (lncRNAs) has only recently been recognized. Technical innovations such as the super high-resolution tiling array and deep sequencing technology have indicated their importance. It has been proposed that lncRNAs such as *HOTAIR* are involved in the recruitment of chromatin modifiers to the target genes. The lncRNA *ANRIL* has been reported to be associated with a Polycomb complex, recruiting it to the target gene *INK4* locus where it suppresses transcription *via* histone modification. Other lncRNAs such as *Kcnq1ot1*, *AIR* and *Xist* have also been found to recruit chromatin modifiers to their target loci. In this review, we discuss the function of lncRNAs such as *HOTAIR*, *ANRIL*, *Kcnq1ot1*, and *Xist* which recruit chromatin modifiers to target genes and discuss their involvement in cancer development and aggressiveness, and other cell fate determination.

**Keywords:** lncRNA, *HOTAIR*, *ANRIL*, *Kcnq1ot1*, *Xist*, polycomb, *INK4* locus, human cancers.

## 1. LONG NON-CODING RNA RECRUITING CHROMATIN MODIFIERS

The eukaryotic genome contains various types of RNAs, mRNA, tRNA, rRNA, snRNA, snoRNA, scaRNA, miRNA, piRNA, siRNA and long non-coding RNAs (lncRNAs/lincRNAs). Many reports have indicated that miRNAs contribute to various types of cell fate determination including cancer development and aggressiveness [1-3]. Recent progress in mass scale transcriptome analysis using the super high-resolution tiling array and deep sequencing technology has revealed that a large number of lncRNAs are transcribed in eukaryotes [4]. Chang's group in Stanford University School of Medicine, USA [5] identified the novel lncRNA *HOTAIR* that is located in the *HOX* gene locus. They found that *HOTAIR* binds to the Polycomb group (PcG) complex and recruits it to the target genes. As a result, histone modification of the chromatin is promoted to regulate transcription of the gene. The PcG contributes to the epigenetic regulation of *HOX* gene cluster transcription by forming Polycomb repressive complex 1 (PRC1) and 2 (PRC2). PcG participates in histone H3K27 methylation as the PRC2 complex and, following histone H2AK119 monoubiquitylation, as the PRC1 complex in the target locus; thereby, the transcriptional repression status of the target gene is promoted and maintained [6]. Subsequently, it has been reported that several of the known lncRNAs such as *Xist*, *Air* and *Kcnq1ot1* also associate with chromatin modifiers including PcG and H3K9 methyltransferase G9a, recruiting them to the target loci [7-10] Fig. (**1A**). Moreover, our group [11] and Yap's groups in Mount Sinai School of Medicine, USA [12] reported that *ANRIL* (antisense noncoding RNA in the INK4 locus) binds to PcG and recruits it to the *INK4* locus which has two cyclin-dependent kinase (CDK) inhibitor genes, *p15* and *p16*, and *ARF* (alternative reading frame different from *p16*) which uses the same exon as the *p16* gene [13] Fig. (**1B**), thereby suppressing transcription of both *p15* and *p16* but not *ARF via* histone modifications in the chromatin. These findings changed perceptions of the roles of the lncRNAs, as they may be generally involved in cancer development and cell fate determination through recruiting chromatin modifiers.

## 2. *HOTAIR*

*HOX* genes are clustered in the vertebrate genome and play important roles in the determination of axis and metamere in embryogenesis. Rinn *et al.* identified 231 ncRNA in human that were transcribed from the four *HOX* gene clusters using the super high-resolution tiling array [5]. Among them, they focused on a novel lncRNA *HOTAIR* (*HOX* antisense intergenic RNA) that is located in the border region between two chromatin domains in the *HOXC* gene that are distinguished by their level of H3K27-methylation. *HOTAIR* is highly conserved in vertebrates. It is transcribed from the *HOXC* genes, spliced to 2.2 kb and a poly (A) tail is added. Interestingly, *HOTAIR* is not involved in the transcription of the *HOXC* genes; rather, it regulates the transcription of the *HOXD* genes in a trans-acting manner. Rinn *et al.* also demonstrated that depletion of *HOTAIR* decreased the recruitment of SUZ12, a component of the PRC2 complex, to *HOXD* genes [5] Fig. (**1A**). The results of both an RNA immunoprecipitation (RIP) assay and a pull-down assay indicated that *HOTAIR* bound directly to the PRC2 complex. Therefore, these workers concluded that *HOTAIR* binds

*Address correspondence to this author at the Department of Molecular Biology, Hamamatsu University School of Medicine, 1-20-1 Handayama, Higashi-ku, Hamamatsu 431-3125, Japan; Tel/Fax: +81-53-434-2322; E-mail: kitamasa@hama-med.ac.jp

1873-5592/12 $58.00+.00 

to and recruits PRC2 to the *HOXD* locus on a different chromosome than the *HOXC* locus that encodes it, resulting in the repression of transcription of the *HOXD* genes. Recently, it has been reported that H3K27 methyltransferase EZH2, a component of PRC2, binds directly to *HOTAIR* and the phosphorylation of Thr345 in EZH2 by cyclin-dependent kinase 1 (CDK1) enhances binding of EZH2 to *HOTAIR* [14]. Moreover, it has been suggested that *HOTAIR* binds not only to PRC2, but also to LSD1, a histone H3K4 demethylase [15]. Therefore, *HOTAIR* functions as a scaffold for chromatin modifiers to recruit them to the HOX genes.

*HOTAIR* has also been reported to be involved in human cancers [16-21]. The overexpression of *HOTAIR* has been found in 10% of human breast cancers. Furthermore, the expression rates of *HOTAIR* in primary breast tumor have been correlated with metastasis and poor prognosis (Table 1). It has been suggested that *HOTAIR* promotes genome-wide rearrangements of PRC2 recruitment to mediate histone H3K27 methylation and that it participates in the suppression of the tumor suppressor gene and the induction of the metastasis promoting gene [16, 17]; thereby, tumor development and metastasis may be promoted. Thus, *HOTAIR* may be associated not only with cancers but also with other diseases *via* reprogramming of the genome.

### 3. *ANRIL*

The *INK4* locus genes such as *p15*, *p16*, and *ARF* are important for tumor suppression because they control two major tumor suppressor pathways, the RB and p53 pathways [22, 23]. It had been suggested that PcG binds to the *INK4* locus thereby suppressing transcription *via* histone H3K27 methylation [24]. Moreover, our group [11] and Yap *et al.* [12] found that *ANRIL* represses the transcription of the *INK4* locus Fig. (**1B**). We found that the depletion of *ANRIL* by short hairpin RNA (shRNA) decreases the recruitment of SUZ12, a component of the PRC2 complex, to the *INK4* locus [11] Fig. (**1C**). Our results also indicated that depletion of *ANRIL* promotes the expression of the *p15* and *p16* genes and induces senescence-associated beta-galactosidase in WI38 human fibroblasts. On the other hand, Yap *et al.* found that *ANRIL* binds to CBX7, a component of the PRC1 complex, in the chromatin fraction and recruits PRC1 to the *INK4* locus [12]. We suggest, therefore, that *ANRIL* may bind to the PRC2 complex to recruit it to the *INK4* locus; then, histone H3K27 methylation (M) is mediated by EZH2 in the PRC2 complex. Next, the PRC2 with *ANRIL* is recognized by CBX7 and the PRC1 complex is recruited to the region and histone H2AK119 mono-ubiquitylation (Ub) is induced to repress transcription of the *INK4* locus Fig. (**1C**). It has been reported that *p16* is strongly associated with cellular senescence [25, 26]. These data suggested that *ANRIL* is involved not only in cell growth but also in the suppression of premature senescence *via* negative regulation of the *INK4* locus by the recruitment of PRC1 and PRC2. Common disease genome-wide association studies (GAWS) suggested that polymorphisms in the *ANRIL* locus may be associated with atherosclerosis, coronary disease, intracranial aneurysm and type 2 diabetes [27-29]. It has been suggested that single-nucleotide polymorphisms (SNPs) may induce *p15/p16* and promote senescence in tissues [29]. *ANRIL* has also been reported that its deletion and polymorphism are associated with melanoma and Philadelphia positive acute lymphoblastic leukemia, respectively [30, 31]. Furthermore, polymor-

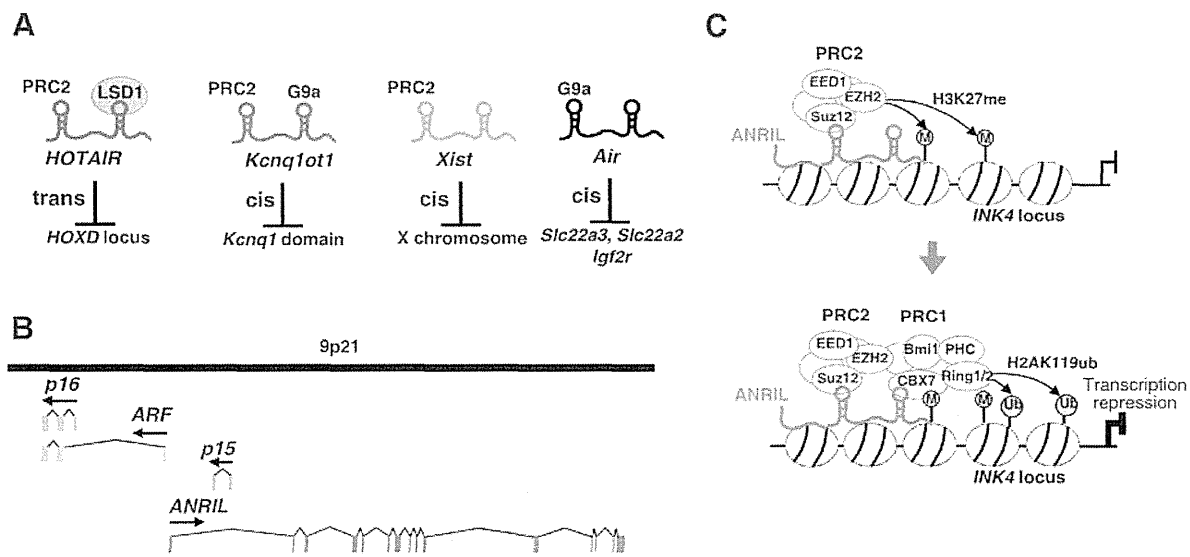


**Fig. (1).** Models showing the proposed mechanisms of action of some of the lncRNAs. **A**. Binding of *HOTAIR*, *Kcnq1ot1*, *Xist* and *Air* to chromatin modifiers. *HOTAIR* binds to PRC2 and LSD1 to repress the transcription of the *HOXD* locus in a trans-acting manner. *Kcnq1ot1* binds to PRC2 and G9a to repress the transcription of the *Kcnq1* domain including $p57^{Kip2}$ in a cis-acting manner. *Xist* binds to PRC2 to participate in X-chromosome inactivation in a cis-acting manner. *Air* binds to G9a to repress the transcription of the indicated genes in a cis-acting manner. **B**. Exon-intron structures of *p15*, *p16* and *ARF* in the human chromosome 9p21 *INK4* locus. The colored blocks represent the exons; the black lines represent the introns; and the arrows indicate the transcription direction. **C**. Model of *ANRIL* mediated repression of the *INK4* locus. *ANRIL* binds to the PRC2 complex to recruit it to the *INK4* locus. Then histone H3K27 methylation (M) is mediated by EZH2 in the PRC2 complex with *ANRIL*, which is recognized by CBX7 to recruit the PRC1 complex to the region. Thereby histone H2AK119 mono-ubiquitylation (Ub) is induced to repress the transcription of *INK4*.

phism on the intron 3 of *ANRIL*, which is correlated with reduced expression of *ANRIL* and increased expression of p15 and p16, is associated with plexiform neurofibroma (PNF) susceptibility [32] (Table 1). Because the *INK4* locus plays a critical role in tumor suppression by regulating the RB and p53 pathways, the abrogation of its expression by *ANRIL* may be involved in many more kinds of cancers than has been reported so far.

### 4. *Kcnq1ot1*

The *Kcnq1* domain is maternally expressed as an imprinting gene. *Kcnq1ot1* is paternally expressed as the antisense RNA of the *Kcnq1* domain containing *Kcnq1* and $p57^{Kip2}$. It has been proposed that *Kcnq1ot1* is a recruiter that associates with the chromatin modifiers PRC2 and G9a to recruit it to the *Kcnq1* domain; thereby, the transcription of *Kcnq1* and $p57^{Kip2}$ is epigenetically suppressed as an imprinting gene in the paternal chromosome [33-36]. There are several reports that *Kcnq1ot1* is involved in the Beckwith-Wiedemann syndrome *via* regulation of the *Kcnq1* domain [37, 38]. In addition, it has been suggested that *Kcnq1ot1* may be associated with the development of cancers such as breast cancers, colorectal cancers and pediatric adrenal tumors [39-41] (Table 1).

### 5. *Xist/XIST*

*Xist* is a specific transcript from the future inactive X chromosome (Xi). *Xist* encodes a lnc RNA and its product accumulates to the future Xi where it initiates X chromosome inactivation. X inactivation is a process that equalizes the dosage of X-linked genes between females (XX) and males (XY), observed in placental mammals. When *Xist* RNA accumulates on the future Xi, it recruits repressive histone modifications such as H3K27me3, catalyzed by PRC2, and H2AK119ub, catalyzed by PRC1, on the future Xi [42]. The 5' region of *Xist* RNA contains a repeat A element motif consisting of 7–8 repeats that is required for gene silencing of the X-linked genes [43]. The mechanism by which *Xist* recruits silencing complexes such as PRC2 and PRC1 is not well determined. However, the direct association of the A repeat with PRC2 has been proposed [7, 44, 45].

Precise dosage compensation is required for normal development in mammals. In the inner cell mass (ICM) of female mouse blastocysts, both the maternal and the paternal X chromosomes were found to be active [46-48]. Undifferentiated female mouse embryonic stem cells (ESC) derived from the ICM, were reported to maintain two active X chromosomes under well-optimized culture conditions [49]. Two active X chromosomes (Xa) have also been maintained in mouse induced pluripotent stem cells (iPSC) during its culture [50]. These findings indicate that dosage compensation is not required for maintaining pluripotent cells such as ESC and iPSC. However, dosage compensation is definitely required for normal development at least in extraembryonic lineages. Reduced *Xist* expression from the paternal X chromosome by targeted disruption of the *Xist* gene [51] or overexpression of *Tsix*, an *Xist* repressor [52] has been reported to evoke embryonic lethality because of failure of normal development in extraembryonic lineages. A recent report suggested that the progenitor of extraembryonic ectoderm (ExE) especially requires dosage compensation for its cell fate. In these cells, expression of Cdx2, the transcriptional regulator required for maintaining ExE in a progenitor state, was lost owing to loss of dosage compensation [53]. Whether dosage compensation is required for normal development in all differentiated cell lineages, including the embryonic lineages is yet to be elucidated.

The function of *XIST* in human cancer development has been reviewed previously [54, 55]. Several potential oncogenic genes including tumor suppressor genes and oncogenes have been identified on the X chromosome in human [56]. The dysregulation of *XIST* that might induce loss or gain of a functional X chromosome can affect tumorgenesis through either the loss of tumor suppressor genes or the gain of increasing the doze of oncogenes from the X chromosome. Indeed, the dysregulation of *XIST* expression, such as ectopic

**Table 1. Representative lncRNAs Involved in Cancer and Cell Fate**

| lncRNA | Target Gene | Function | Associated Molecule | Association with Human Cancers | References |
|---|---|---|---|---|---|
| *HOTAIR* | *Hox locus* | *HOX* gene repression | PRC1/2 | Breast, hepatocellular, colon, pancreatic cancer | [5, 6, 16-21] |
| *ANRIL* | *INK4 locus* | *p15/p16* gene repression, senescence inhibition | PRC1/2 | Melanoma, Philadelphia positive acute lymphoblastic leukemia, plexiform neurofibroma | [11, 12, 27-32] |
| *Kcnq1ot1* | *Kcnq1, p57* | *Kcnq1* and *p57* repression | PRC2, G9a | Breast, colon, pediatric adrenal cancer | [33-41] |
| *Xist/XIST* | X chromosome | X chromosome inactivation | PRC2 | Breast, ovarian, cervical, prostate cancer | [42-62] |
| *PANDA* | *BIK, FAS* | Apoptosis gene repression | NF-YA | Unknown | [63] |
| *MALAT1* | - | Splicing regulation, cell motility gene promotion | Splicing component | Lung, cervical, hepato- cellular carcinomas etc | [64-73] |
| $ncRNA_{CCD1}$ | *CyclinD1* | *CyclinD1* gene repression | TLS | Unknown | [74-77] |

*XIST* expression from the Xa, has been observed in some breast cancer cells [57] and the loss of *XIST* expression from the Xi has been reported in female breast, ovarian and cervical cancer cell lines [58, 59]. Moreover, changing the copy number of either the Xa or the Xi has also been observed in several cancer cells [55]. However, whether aberrant *XIST* expression or copy number of the X chromosome is the cause or consequence of the tumorgenesis is yet to be explained because both epigenetic and genetic instabilities are commonly observed in cancers. Experimental confirmation of whether forced expression or conditional deletion of the *Xist* gene can affect tumorgenesis, might provide the evidence with which to address this question.

Although the function of *XIST* in tumorgenesis is still controversial, the expression or methylation levels of the *XIST* gene can be used as a maker for tumors. The *XIST* gene on the Xa from males and females is methylated to repress the *XIST* expression. However, male germ tumor cells showed ectopic *XIST* RNA expression that was confirmed by the polymerase chain reaction (PCR) [60]. In addition to the expression of the *XIST* RNA, the *XIST* gene was shown to be unmethylated in testicular germ cell tumors (TGCTs) [60] and in prostate cancer [62]. These findings strongly indicated that the methylated status of *XIST* can be used as a marker for tumor diagnosis. This contribution could have a positive impact on human health.

## 6. OTHER lncRNAs INVOLVED IN CELL CYCLE AND CANCER

Many reports have linked lncRNAs to cancer development and cell fate determination. Apart from *HOTAIR*, *ANRIL*, *Kcnq1ot1*, and *Xist* (discussed above), other lncRNAs including *PANDA*, $ncRNA_{CCND1}$ and *MALAT1* (Table **1**), act with chromatin modifiers through mechanisms that are different from the mechanisms used by *HOTAIR*, *ANRIL*, and *Kcnq1ot1*.

*PANDA* (p21 associated ncRNA DNA damage activated) is one of the p21 promoter-derived transcripts that are induced by DNA damage [63]. *PANDA* binds to and inhibits the NF-YA transcription factor, which limits the expression of proapoptotic genes such as FAS and BIK and results in the repression of apoptosis. *PANDA* is selectively induced in metastatic ductal carcinomas but not in normal breast tissue. The results suggest that abnormal overexpression of *PANDA* may suppress apoptosis by DNA damage, which will accumulate and push the genome toward carcinogenesis.

*MALAT1* (metastasis-associated lung adenocarcinoma transcript 1) was found to be associated with metastasis and poor prognosis in various human cancers [64-71]. Overexpression of *MALAT1* has been reported in lung cancers, cervical cancers and hepatocellular carcinomas (Table **1**). It has been suggested that *MALAT1* is involved in the regulation of alternative splicing of cancer-associated genes [72, 73]. However, so far, little is known about the function of *MALAT1*.

$ncRNA_{CCND1}$ is transcribed from the upstream region of the cyclin D1 gene in a DNA damage-dependent manner [74]. It associates with and recruits TLS (translocated in liposarcoma) [75], an RNA binding protein, to the cyclin D1 promoter, thereby inhibiting the interaction of the coactivator CBP with the cyclin D1 promoter and preventing cyclin D1 transcription [76, 77]. Although little is known about the role of $ncRNA_{CCND1}$, it is possible to speculate that it may be associated with carcinogenesis or cancer development because the overexpression of cyclin D1 is known to be closely associated with breast cancer development.

## PERSPECTIVES

Recent studies have suggested that functional lncRNAs make up a large proportion of the lncRNAs. Moreover, there is evidence that *HOTAIR*, *Kcnq1ot1* and *MALAT1* behave as oncogenes in cancer development and it has been suggested that *ANRIL*, *Xist* and *PANDA* also have oncogenic properties. These lncRNAs may be novel candidate molecular targets for cancer therapy or diagnosis. Further, if the interactions between these lncRNAs and their effecter molecules can be specifically inhibited by a small molecule, this molecule may become a novel anticancer drug. Considering the recent progress in lncRNA research, many currently unknown lncRNAs that have a functional role in various human diseases may be identified and developed as novel drug targets.

## CONFLICT OF INTEREST

The authors confirm that this article content has no conflicts of interest.

## ACKNOWLEDGEMENT

Declared none.

## REFERENCES

[1] Stefani G, Slack FJ. Small non-coding RNAs in animal development. Nat Rev Mol Cell Biol 2008; 9: 219-30.

[2] Sato F, Tsuchiya S, Meltzer SJ, Shimizu K. MicroRNAs and epigenetics. FEBS Journal 2011; 278: 1598-609.

[3] Iorio MV, Croce CM. MicroRNA dysregulation in cancer: diagnostics, monitoring and therapeutics. A comprehensive review. EMBO Mol Med 2012; 4: 143-59. 6,

[4] Carninci P, Kasukawa T, Katayama S, *et al.* FANTOM Consortium; RIKEN Genome Exploration Research Group and Genome Science Group (Genome Network Project Core Group). The transcriptional landscape of the mammalian genome. Science 2005; 309: 1559-63.

[5] Rinn JL, Kertesz M, Wang JK, *et al.* Functional demarcation of active and silent chromatin domains in human HOX loci by noncoding RNAs. Cell 2007; 129: 1311-23.

[6] Wang L, Brown JL, Cao R, Zhang Y, Kassis JA, Jones RS. Hierarchical recruitment of polycomb group silencing complexes. Mol Cell 2004; 14: 637-46.

[7] Zhao J, Sun BK, Erwin JA, Song JJ, Lee JT. Polycomb proteins targeted by a short repeat RNA to the mouse X chromosome. Science 2008; 322: 750-6.

[8] Nagano T, Mitchell JA, Sanz LA, *et al.* The Air noncoding RNA epigenetically silences transcription by targeting G9a to chromatin. Science 2008; 322: 1717-20.

[9] Saxena A, Carninci P. Long non-coding RNA modifies chromatin: epigenetic silencing by long non-coding RNAs. Bioessays 2011; 33: 830-9.

[10] Hung T, Chang HY. Long noncoding RNA in genome regulation: prospects and mechanisms. RNA Biol 2010; 7: 582-5.

[11] Kotake Y, Nakagawa T, Kitagawa K, *et al.* Long non-coding RNA ANRIL is required for the PRC2 recruitment to and silencing of p15(INK4B) tumor suppressor gene. Oncogene 2011; 30: 1956-62.

[12] Yap KL, Li S, Muñoz-Cabello AM, *et al.* Molecular interplay of the noncoding RNA ANRIL and methylated histone H3 lysine 27

by polycomb CBX7 in transcriptional silencing of INK4a. Mol Cell 2010; 38: 662-74.

[13] Gil J, Peters G. Regulation of the INK4b-ARF-INK4a tumour suppressor locus: all for one or one for all. Nat Rev Mol Cell Biol 2006; 7: 667-77.

[14] Kaneko S, Li G, Son J, *et al.* Phosphorylation of the PRC2 component Ezh2 is cell cycle-regulated and up-regulates its binding to ncRNA. Genes Dev 2010; 24: 2615-20.

[15] Tsai MC, Manor O, Wan Y, *et al.* Long noncoding RNA as modular scaffold of histone modification complexes. Science 2010; 329: 689-93.

[16] Wan Y, Chang HY. HOTAIR: Flight of noncoding RNAs in cancer metastasis. Cell Cycle 2010; 9: 3391-2.

[17] Gupta RA, Shah N, Wang KC, *et al.* Long non-coding RNA HOTAIR reprograms chromatin state to promote cancer metastasis. Nature 2010; 464: 1071-6.

[18] Yang Z, Zhou L, Wu LM, *et al.* Overexpression of long non-coding RNA HOTAIR predicts tumor recurrence in hepatocellular carcinoma patients following liver transplantation. Ann Surg Oncol 2011; 18: 1243-50.

[19] Kogo R, Shimamura T, Mimori K, *et al.* Long noncoding RNA HOTAIR regulates polycomb-dependent chromatin modification and is associated with poor prognosis in colorectal cancers. Cancer Res 2011; 71: 6320-6.

[20] Niinuma T, Suzuki H, Nojima M, *et al.* Upregulation of miR-196a and HOTAIR drive malignant character in gastrointestinal stromal tumors. Cancer Res 2012; 72: 1126-36.

[21] Kim K, Jutooru I, Chadalapaka G, *et al.* HOTAIR is a negative prognostic factor and exhibits pro-oncogenic activity in pancreatic cancer. Oncogene 2012. doi: 10.1038/onc.2012.193

[22] Sherr CJ, McCormick F. The RB and p53 pathways in cancer. Cancer Cell 2002; 2: 103-12.

[23] Kitagawa K, Kotake Y, Kitagawa M. Ubiquitin-mediated control of oncogene and tumor suppressor gene products. Cancer Sci 2009; 100: 1374-81.

[24] Kotake Y, Cao R, *Viat*our P, Sage J, Zhang Y, Xiong Y. pRB family proteins are required for H3K27 trimethylation and Polycomb repression complexes binding to and silencing p16INK4a tumor suppressor gene. Genes Dev 2007; 21: 49-54.

[25] Jacobs JJ, Kieboom K, Marino S, DePinho RA, van Lohuizen M. The oncogene and Polycomb-group gene bmi-1 regulates cell proliferation and senescence through the ink4a locus. Nature 1999; 397: 164-8.

[26] Rayess H, Wang MB, Srivatsan ES. Cellular senescence and tumor suppressor gene p16. Int J Cancer 2012; 130:1715-25.

[27] Broadbent HM, Peden JF, Lorkowski S, *et al.* Susceptibility to coronary artery disease and diabetes is encoded by distinct, tightly linked SNPs in the ANRIL locus on chromosome 9p. Hum Mol Genet 2008; 17: 806-14.

[28] Holdt LM, Beutner F, Scholz M, *et al.* ANRIL expression is associated with atherosclerosis risk at chromosome 9p21. Arterioscler Thromb Vasc Biol 2010; 30: 620-7.

[29] Cunnington MS, Santibanez Koref M, Mayosi BM, Burn J, Keavney B. Chromosome 9p21 SNPs Associated with Multiple Disease Phenotypes Correlate with ANRIL Expression. PLoS Genet 2010; 6: e1000899.

[30] Pasmant E, Laurendeau I, Héron D, Vidaud M, Vidaud D, Bièche I. Characterization of a germ-line deletion, including the entire INK4/ARF locus, in a melanoma-neural system tumor family: identification of ANRIL, an antisense noncoding RNA whose expression coclusters with ARF. Cancer Res 2007; 67: 3963-9.

[31] Iacobucci I, Sazzini M, Garagnani P, *et al.* A polymorphism in the chromosome 9p21 ANRIL locus is associated to Philadelphia positive acute lymphoblastic leukemia. Leuk Res 2011; 35: 1052-9.

[32] Pasmant E, Sabbagh A, Masliah-Planchon J, *et al.*; NF France Network. Role of noncoding RNA ANRIL in genesis of plexiform neurofibromas in neurofibromatosis type 1. J Natl Cancer Inst 2011; 103: 1713-22.

[33] Pandey RR, Mondal T, Mohammad F, *et al.* Kcnq1ot1 antisense noncoding RNA mediates lineage-specific transcriptional silencing through chromatin-level regulation. Mol Cell 2008; 32: 232-46.

[34] Mager J, Montgomery ND, de Villena FP, Magnuson T. Genome imprinting regulated by the mouse Polycomb group protein Eed. Nat Genet 2003; 33: 502-7.

[35] Umlauf D, Goto Y, Cao R, *et al.* Imprinting along the Kcnq1 domain on mouse chromosome 7 involves repressive histone methylation and recruitment of Polycomb group complexes. Nat Genet 2004; 36: 1296-300.

[36] Wagschal A, Sutherland HG, Woodfine K, *et al.* G9a histone methyltransferase contributes to imprinting in the mouse placenta. Mol Cell Biol 2008; 28: 1104-13.

[37] Arima T, Kamikihara T, Hayashida T, *et al.* ZAC, LIT1 (KCNQ1OT1) and p57KIP2 (CDKN1C) are in an imprinted gene network that may play a role in Beckwith-Wiedemann syndrome. Nucleic Acids Res. 2005; 33: 2650-60.

[38] Higashimoto K, Soejima H, Saito T, Okumura K, Mukai T. Imprinting disruption of the CDKN1C/KCNQ1OT1 domain: the molecular mechanisms causing Beckwith-Wiedemann syndrome and cancer. Cytogenet Genome Res 2006; 113: 306-12.

[39] Nakano S, Murakami K, Meguro M, *et al.* Expression profile of LIT1/KCNQ1OT1 and epigenetic status at the KvDMR1 in colorectal cancers. Cancer Sci 2006; 97: 1147-54.

[40] Rodriguez BA, Weng YI, Liu TM, *et al.* Estrogen-mediated epigenetic repression of the imprinted gene cyclin-dependent kinase inhibitor 1C in breast cancer cells. Carcinogenesis 2011; 32: 812-21.

[41] Wijnen M, Alders M, Zwaan CM, Wagner A, van den Heuvel-Eibrink MM. KCNQ1OT1 hypomethylation: A Novel disguised genetic predisposition in sporadic pediatric adrenocortical tumors? Pediatr Blood Cancer 2011. doi: 10.1002/pbc.23398.

[42] Wutz A. Gene silencing in X-chromosome inactivation: advances in understanding facultative heterochromatin formation. Nat Rev Genet 2011; 12: 542-53.

[43] Wutz A, Rasmussen TP, Jaenisch R. Chromosomal silencing and localization are mediated by different domains of Xist RNA. Nat Genet 2002; 30: 167-74.

[44] Duszczyk MM, Wutz A, Rybin V, Sattler M. The Xist RNA A-repeat comprises a novel AUCG tetraloop fold and a platform for multimerization. RNA 2011; 17: 1973-82.

[45] Maenner S, Blaud M, Fouillen L, *et al.* 2-D structure of the A region of Xist RNA and its implication for PRC2 association. PLoS Biol 2010; 8: e1000276.

[46] Huynh KD, Lee JT. Inheritance of a pre-inactivated paternal X chromosome in early mouse embryos. Nature 2003; 426: 857-62.

[47] Okamoto I, Otte AP, Allis CD, Reinberg D, Heard E. Epigenetic dynamics of imprinted X inactivation during early mouse development. Science 2004; 30: 644-9.

[48] Mak W, Nesterova TB, de Napoles M, *et al.* Reactivation of the paternal X chromosome in early mouse embryos. Science 2004; 303: 666-9.

[49] Barakat TS, Gribnau J. X chromosome inactivation in the cycle of life. Development 2012; 139: 2085-9.

[50] Stadtfeld M, Maherali N, Breault DT, Hochedlinger K. Defining molecular cornerstones during fibroblast to iPS cell reprogramming in mouse. Cell Stem Cell 2008; 2: 230-40.

[51] Marahrens Y, Panning B, Dausman J, Strauss W, Jaenisch R. Xist-deficient mice are defective in dosage compensation but not spermatogenesis. Genes Dev 1997; 11: 156-66.

[52] Ohhata T, Senner CE, Hemberger M, Wutz A. Lineage-specific function of the noncoding Tsix RNA for Xist repression and Xi reactivation in mice. Genes Dev 2011; 25: 1702-15.

[53] Mugford JW, Yee D, Magnuson T. Failure of extra-embryonic progenitor maintenance in the absence of dosage compensation. Development 2012; 139: 2130-8.

[54] Agrelo R, Wutz A. ConteXt of change--X inactivation and disease. EMBO Mol Med 2010; 2: 6-15.

[55] Weakley SM, Wang H, Yao Q, Chen C. Expression and function of a large non-coding RNA gene XIST in human cancer. World J Surg 2011; 35: 1751-6.

[56] Spatz A, Borg C, Feunteun J. X-chromosome genetics and human cancer. Nat Rev Cancer 2004; 4: 617-29.

[57] Sirchia SM, Tabano S, Monti L, *et al.* Misbehaviour of XIST RNA in breast cancer cells. PLoS One 2009; 4: e5559.

[58] Kawakami T, Zhang C, Taniguchi T, *et al.* Characterization of loss-of-inactive X in Klinefelter syndrome and female-derived cancer cells. Oncogene 2004; 23: 6163-9.

[59] Benoît MH, Hudson TJ, Maire G, *et al.* Global analysis of chromosome X gene expression in primary cultures of normal ovarian surface epithelial cells and epithelial ovarian cancer cell lines. Int J Oncol 2007; 30: 5-17.

[60] Looijenga LH, Gillis AJ, van Gurp RJ, Verkerk AJ, Oosterhuis JW. X inactivation in human testicular tumors. XIST expression and

androgen receptor methylation status. Am J Pathol 1997; 151: 581-90.

[61] Kawakami T, Okamoto K, Ogawa O, Okada Y. XIST unmethylated DNA fragments in male-derived plasma as a tumour marker for testicular cancer. Lancet 2004; 363: 40-2.

[62] Song MA, Park JH, Jeong KS, Park DS, Kang MS, Lee S. Quantification of CpG methylation at the 5'-region of XIST by pyrosequencing from human serum. Electrophoresis 2007; 28: 2379-84.

[63] Hung T, Wang Y, Lin MF, *et al.* Extensive and coordinated transcription of noncoding RNAs within cell-cycle promoters. Nat Genet 2011; 43: 621-9.

[64] Lin R, Roychowdhury-Saha M, Black C, *et al.* Control of RNA processing by a large non-coding RNA over-expressed in carcinomas. FEBS Lett 2011; 585: 671-6.

[65] Xu C, Yang M, Tian J, Wang X, Li Z. MALAT-1: a long noncoding RNA and its important 3' end functional motif in colorectal cancer metastasis. Int J Oncol 2011; 39: 169-75.

[66] Schmidt LH, Spieker T, Koschmieder S, *et al.* The long noncoding MALAT-1 RNA indicates a poor prognosis in non-small cell lung cancer and induces migration and tumor growth. J Thorac Oncol 2011; 6: 1984-92.

[67] Lin R, Maeda S, Liu C, Karin M, Edgington TS. A large noncoding RNA is a marker for murine hepatocellular carcinomas and a spectrum of human carcinomas. Oncogene 2007; 26: 851-8.

[68] Wheeler TM, Leger AJ, Pandey SK, *et al.* Targeting nuclear RNA for *in vivo* correction of myotonic dystrophy. Nature 2012; 488: 111-5.

[69] Zhang B, Arun G, Mao YS, *et al.* The lncRNA Malat1 Is Dispensable for Mouse Development but Its Transcription Plays a cis-Regulatory Role in the Adult. Cell Rep 2012; 2: 111-23.

[70] Eißmann M, Gutschner T, Hämmerle M, *et al.* Loss of the abundant nuclear non-coding RNA MALAT1 is compatible with life and development. RNA Biol 2012; 9(8). [Epub ahead of print].

[71] Schmidt LH, Spieker T, Koschmieder S, *et al.* The long noncoding MALAT-1 RNA indicates a poor prognosis in non-small cell lung cancer and induces migration and tumor growth. J Thorac Oncol 2011; 6: 1984-92.

[72] Wilusz JE, Freier SM, Spector DL. 3' end processing of a long nuclear-retained noncoding RNA yields a tRNA-like cytoplasmic RNA. Cell 2008; 135: 919-32.

[73] Miyagawa R, Tano K, Mizuno R, *et al.* Identification of cis- and trans-acting factors involved in the localization of MALAT-1 noncoding RNA to nuclear speckles. RNA 2012; 18: 738-51.

[74] Wang X, Arai S, Song X, *et al.* Induced ncRNAs allosterically modify RNA-binding proteins in cis to inhibit transcription. Nature 2008; 454: 126-30.

[75] Haile S, Lal A, Myung JK, Sadar MD. FUS/TLS is a co-activator of androgen receptor in prostate cancer cells. PLoS One 2011; 6: e24197.

[76] Kurokawa R. Promoter-associated long noncoding RNAs repress transcription through a RNA binding protein TLS. Adv Exp Med Biol 2011; 722: 196-208.

[77] Oyoshi T, Kurokawa R. Structure of noncoding RNA is a determinant of function of RNA binding proteins in transcriptional regulation. Cell Biosci 2012; 2: 1.

**Received: August 27, 2012** **Revised: September 05, 2012** **Accepted: September 14, 2012**

Science Translational Medicine AAAS

**Decreased Tonic Inhibition in Cerebellar Granule Cells Causes Motor Dysfunction in a Mouse Model of Angelman Syndrome**
Kiyoshi Egawa *et al.*
*Sci Transl Med* **4**, 163ra157 (2012);
DOI: 10.1126/scitranslmed.3004655

Editor's Summary

**Elucidating the Mechanism of Ataxia in Angelman Syndrome**

Angelman syndrome is a neurodevelopmental disorder caused by loss of the ubiquitin E3 ligase Ube3a. A variety of symptoms, including severe developmental delay, speech impairment, epilepsy, and movement and balance problems, are associated with Angelman syndrome. In a new study, Egawa *et al.* investigate electrophysiological features of cerebellar dysfunction in a mouse model of Angelman syndrome. The authors report that extrasynaptic γ-aminobutyric acid type A ($GABA_A$) receptor–mediated tonic inhibition decreases in cerebellar granule cells from the Ube3a-deficient Angelman mice. They then show that, normally, Ube3a binds to GABA transporter 1, a key modulator of extrasynaptic GABA, and controls its degradation in the mouse cerebellum. The Ube3a-deficient mice, however, showed a surplus of GABA transporter 1, resulting in decreased GABA concentrations in the extrasynaptic space and thus decreased tonic inhibition of cerebellar granule cells. Pharmacological compensation of decreased tonic inhibition by administering low doses of THIP, a selective agonist of extrasynaptic $GABA_A$ receptors, alleviated impaired motor function in the Ube3a-deficient mice. Thus, attenuated GABA transporter 1 degradation and a consequent decrease in tonic inhibition of cerebellar granule cells play a key role in the cerebellar dysfunction characteristic of Angelman syndrome. Pharmacologically increasing tonic inhibition with THIP may be a useful strategy for alleviating movement and balance problems in patients with this disease.

RESEARCH ARTICLE

NEURODEGENERATIVE DISEASE

# Decreased Tonic Inhibition in Cerebellar Granule Cells Causes Motor Dysfunction in a Mouse Model of Angelman Syndrome

**Kiyoshi Egawa,[1]*† Kyoko Kitagawa,[2] Koichi Inoue,[1] Masakazu Takayama,[1] Chitoshi Takayama,[3] Shinji Saitoh,[4] Tatsuya Kishino,[5] Masatoshi Kitagawa,[2] Atsuo Fukuda[1]†**

*Angelman syndrome is a neurodevelopmental disorder caused by loss of function of the UBE3A gene encoding a ubiquitin E3 ligase. Motor dysfunction is a characteristic feature of Angelman syndrome, but neither the mechanisms of action nor effective therapeutic strategies have yet been elucidated. We report that tonic inhibition is specifically decreased in cerebellar granule cells of Ube3a-deficient mice, a model of Angelman syndrome. As a mechanism underlying this decrease in tonic inhibition, we show that Ube3a controls degradation of γ-aminobutyric acid (GABA) transporter 1 (GAT1) and that deficiency of Ube3a induces a surplus of GAT1 that results in a decrease in GABA concentrations in the extrasynaptic space. Administering low doses of 4,5,6,7-tetrahydroisothiazolo-[5,4-c]pyridin-3-ol (THIP), a selective extrasynaptic $GABA_A$ receptor agonist, improves the abnormal firing properties of a population of Purkinje cells in cerebellar brain slices and reduces cerebellar ataxia in Ube3a-deficient mice in vivo. These results suggest that pharmacologically increasing tonic inhibition may be a useful strategy for alleviating motor dysfunction in Angelman syndrome.*

## INTRODUCTION

Angelman syndrome is a neurodevelopmental disorder caused by a functional deficit in the brain-specific imprinted gene *UBE3A* (*1*, *2*), which encodes the ubiquitin E3 ligase Ube3a (*3*) [also known as E6-associated protein (E6-AP)]. The major clinical manifestations consist of severe developmental delay, speech impairment, epilepsy, movement and balance problems, and characteristic behavior such as paroxysmal laughter (*4*). The mechanisms underlying Angelman syndrome–associated learning impairments have been revealed progressively (*5*–*7*) since the construction of a mouse model ($Ube3a^{m-/p+}$) by targeted inactivation of maternal *Ube3a* (*2*, *8*).

Abnormal movement and balance are characteristic features of Angelman syndrome that are largely attributed to cerebellar ataxia (*9*, *10*), with about 35% of patients remaining nonambulatory at 5 years (*11*). However, despite its severe impact on patients, the mechanisms underlying the cerebellar ataxia in Angelman syndrome are still not clear. Several investigators have hypothesized that GABAergic dysfunction is involved in the neurological symptoms caused by Ube3a deficiency (*9*, *10*). This is because patients with Angelman syndrome in whom there is deletion of chromosomes containing genes encoding γ-aminobutyric acid type A ($GABA_A$) receptor β3, α5, and γ3 subunits show a more severe phenotype than do patients without these deletions (*11*, *12*). However, paradoxically, the frequency and amplitude of phasic inhibitory postsynaptic currents (IPSCs) are normal in $Ube3a^{m-/p+}$ mice (*7*). These conflicting findings imply that another form of inhibition, for example, tonic inhibition, might be compromised in Ube3a deficiency. Tonic inhibition is mediated by high-affinity, extrasynaptic $GABA_A$ receptors (*13*, *14*) containing α6 and δ subunits that are exclusively expressed in cerebellar granule cells (*15*).

The contribution of tonic inhibition to central nervous system (CNS) diseases is unclear. Recently, gain, rather than loss, of tonic inhibition has been shown to underlie the pathophysiology of epilepsy (*16*) and dysfunction after stroke (*17*), both of which are due to down-regulation of GABA transporters. Studying the mechanisms of GABA transporter regulation is therefore likely to be essential for understanding the pathophysiology of Angelman syndrome. Here, we provide evidence that Ube3a binds to GABA transporter 1 (GAT1) and that Ube3a deficiency causes reduced degradation of GAT1. We further show that decreased concentrations of GABA, leading to decreased tonic inhibition of cerebellar granule cells, are the underlying cause of the cerebellar ataxia in Angelman syndrome.

## RESULTS

### Tonic inhibition is decreased in the cerebellar granule cells of $Ube3a^{m-/p+}$ mice

Recent studies using transgenic mice expressing a Ube3aYFP fusion gene have demonstrated that native Ube3a is maternally expressed in the cerebellar cortex, including the granule cell layer (*18*). Accordingly, we observed positive Ube3a immunoreactivity in the granule cell layer (particularly in presumed Golgi cells) of wild-type but not $Ube3a^{m-/p+}$ mice (fig. S1). Electron microscopic analysis did not reveal any apparent morphological changes in granule cell layer cytoarchitecture or synaptic architecture (fig. S2), indicating a functional rather than a structural disturbance in the mutant cerebellum.

Whole-cell voltage clamp recordings were conducted in cerebellar granule cells of acutely prepared cerebellar brain slices from mice at postnatal day (P) 25 to 28 (Fig. 1A). $GABA_A$ receptor–mediated tonic currents ($I_{tonic}$) decreased by 34.1% in $Ube3a^{m-/p+}$ mice compared

[1]Department of Neurophysiology, Hamamatsu University School of Medicine, Hamamatsu 431-3192, Japan. [2]Department of Molecular Biology, Hamamatsu University School of Medicine, Hamamatsu 431-3192, Japan. [3]Department of Molecular Anatomy, School of Medicine, University of the Ryukyus, Nishihara 903-0215, Japan. [4]Department of Pediatrics and Neonatology, Nagoya City University Graduate School of Medical Sciences, Nagoya 467-8601, Japan. [5]Nagasaki University Center for Frontier Life Sciences, Nagasaki 852-8523, Japan.
*Present address: Department of Neurology, Massachusetts General Hospital, 16th Street, CNY B-114, Charlestown, MA 02114, USA.
†To whom correspondence should be addressed. E-mail: cdh67560@par.odn.ne.jp (K.E.); axfukuda@hama-med.ac.jp (A.F.)

with wild-type mice (Fig. 1, A and C), as did the root mean square noise in the base holding current (Fig. 1D). Although the strength of tonic inhibition has been shown to increase during development (*19*), in $Ube3a^{m-/p+}$ mice the reduction of $I_{tonic}$ and base current noise was sustained into adulthood (Fig. 1, B and D), indicating that the decreased tonic inhibition at P25 to P28 was not a transient phenomenon. Additional in vitro analyses were therefore performed in P25 to P28 mice.

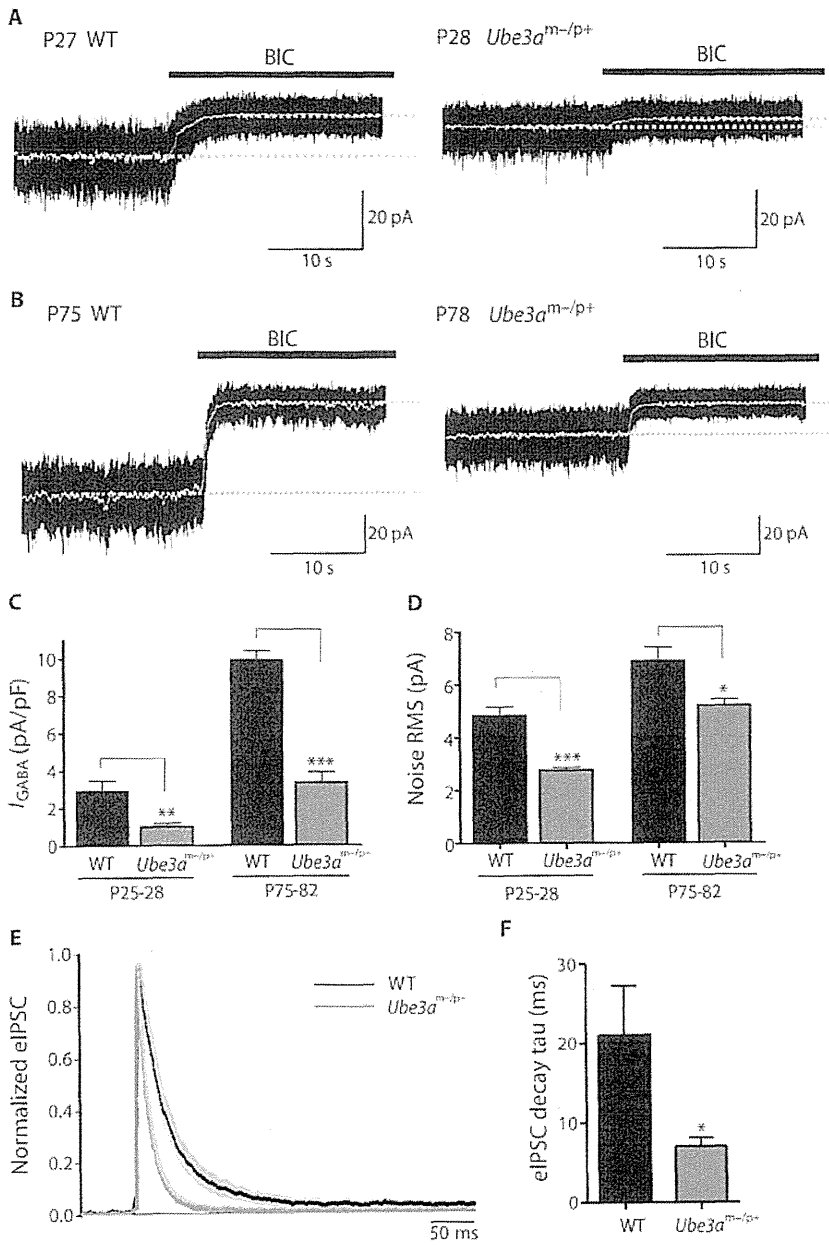


**Fig. 1.** Cerebellar tonic inhibition is decreased in $Ube3a^{m-/p+}$ mice. (**A** and **B**) Representative current traces of cerebellar granule cells from P25 to P28 (A) and P75 to P82 (B) wild-type (WT) and $Ube3a^{m-/p+}$ mice. Tonic $GABA_A$ receptor–mediated current ($I_{GABA}$) was induced by focal application of 20 μM bicuculline (BIC, black bars). To clarify the baseline, a 5-Hz, low pass–filtered overlay is given (gray traces) and extended (dotted gray lines). (**C**) Comparison of $I_{GABA}$ density in WT (P25 to P28: $n = 14$, P75 to P82: $n = 8$) and $Ube3a^{m-/p+}$ (P25 to P28: $n = 15$, P75 to P82: $n = 8$) mice. (**D**) Comparison of root mean square (RMS) current noise of the base holding currents before application of BIC in the same mice as in (C). (**E**) Averaged traces of normalized eIPSCs in cerebellar granule cells from WT (black trace, $n = 9$) and $Ube3a^{m-/p+}$ (red trace, $n = 9$) mice. Pale colors indicate SEM. (**F**) Comparison of the eIPSC decay time constant (tau) shown in (E). $^*P < 0.05$, $^{**}P < 0.01$, $^{***}P < 0.001$, unpaired *t* test. Data are means ± SEM.

Mean spontaneous IPSC (sIPSC) amplitude, rise time, and decay time were not significantly different between $Ube3a^{m-/p+}$ and wild-type cerebellar granule cells ($P = 0.61$, 0.48, and 0.53, respectively; fig. S3, A to D). In accordance with previous reports, sIPSC frequency in cerebellar granule cells was low, usually less than 1 Hz (*19*), and was comparable between $Ube3a^{m-/p+}$ and wild-type mice ($P = 0.69$, Mann-Whitney *U* test; fig. S3E). These results indicate that in contrast to tonic inhibition, phasic inhibition in $Ube3a^{m-/p+}$ mice was not altered. We further evaluated evoked IPSCs (eIPSCs) in cerebellar granule cells. The eIPSC paired-pulse ratios did not significantly differ: interstimulus interval: 50 ms; wild-type: 1.02 ± 0.09, $n = 7$; $Ube3a^{m-/p+}$: 1.00 ± 0.07, $n = 10$; $P = 0.88$. However, the eIPSC decay rate was significantly faster in $Ube3a^{m-/p+}$ mice ($P < 0.05$; Fig. 1, E and F). Because eIPSCs are known to decay more slowly than sIPSCs in cerebellar granule cells owing to activation of extrasynaptic $GABA_A$ receptors (*20*), and because only eIPSC decay rate differed between mouse groups, events mediated by these receptors are likely specifically compromised in $Ube3a^{m-/p+}$ mice.

## Increased GAT1 activity underlies the decreased tonic inhibition in $Ube3a^{m-/p+}$ mice

Down-regulation of extrasynaptic $GABA_A$ receptors is a potential mechanism underlying decreased tonic inhibition. To verify this, we evaluated extrasynaptic $GABA_A$ receptor activation induced by exogenous GABA. Sustained current induced by pressure application with 600 nM GABA ($I_{GABA\ 600\ nM}$), an applied concentration higher than the predicted ambient concentration of GABA in the extrasynaptic space (*21*), was not significantly different between groups ($P = 0.48$), whereas that induced by endogenous ambient GABA was ($I_{tonic}$; Fig. 2, A and B). Plotting the fold increase of $I_{GABA\ 600\ nM}$ against $I_{tonic}$ from both genotypes showed a clear inverse correlation that was well fitted by a Hill equation (Fig. 2B; $R^2 = 0.783$). Because down-regulation of extrasynaptic $GABA_A$ receptors should result in less activation regardless of the source of GABA, these results suggest that the decreased tonic inhibition observed in $Ube3a^{m-/p+}$ mice is caused by lower ambient GABA concentrations rather than receptor down-regulation.

The ambient GABA concentration is tightly regulated by neuronal GAT1 and glial GATs (predominantly GABA transporter 4 in mice), which can take up GABA from the extrasynaptic space (*17*, *22*, *23*). Because maternally expressed Ube3a is not observed in astrocytes (*18*, *24*), we evaluated the effect of GAT1

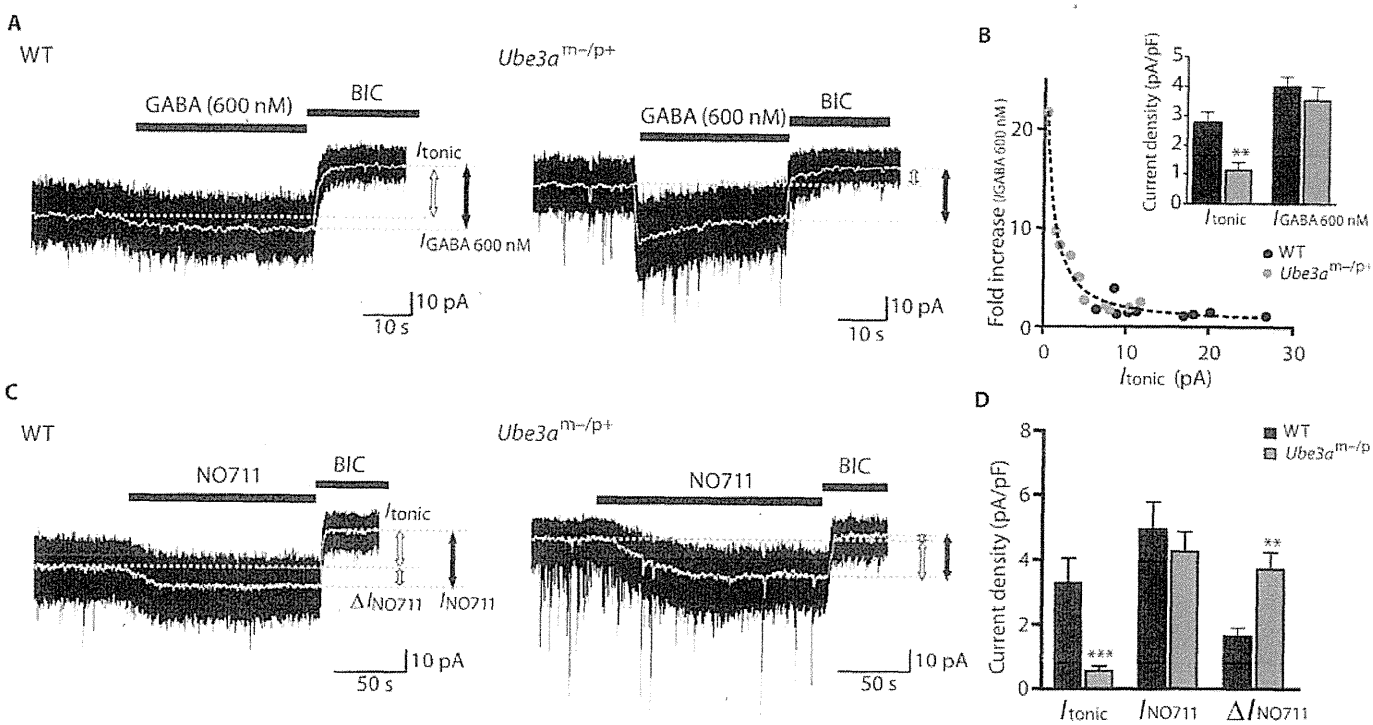


**Fig. 2.** GABA decreases due to increased GAT1 activity underlie the decreased tonic inhibition found in *Ube3a*$^{m-/p+}$ mice. (**A**) Representative traces showing the effects of GABA (600 nM) application on base holding currents. Each baseline is indicated by a dotted line. Tonic holding currents induced by endogenous ($I_{tonic}$) and exogenous GABA ($I_{GABA\ 600\ nM}$) are indicated by thick white and black vertical arrows, respectively. (**B**) The fold increase of $I_{GABA\ 600\ nM}$ against $I_{tonic}$ is plotted for each cerebellar granule cell from WT (black circle) and *Ube3a*$^{m-/p+}$ (red circle) mice. The fitted curve (dotted line) was integrally calculated from WT and *Ube3a*$^{m-/p+}$ mice with a Hill equation. The inset graph shows a comparison of current densities in WT ($n$ = 9, black) and *Ube3a*$^{m-/p+}$ ($n$ = 11, red) mice. (**C**) Representative current traces showing the effect of NO711 on base holding currents. $I_{tonic}$, NO711-induced base holding currents ($I_{NO711}$), and the change in holding currents ($\Delta I_{NO711}$) are indicated by thick white, black, and gray vertical arrows, respectively. (**D**) Comparison of current densities in WT ($n$ = 7, black) and *Ube3a*$^{m-/p+}$ ($n$ = 9, red) mice. $^{**}P < 0.01$, $^{***}P < 0.001$, unpaired $t$ test. Data are means ± SEM.

on tonic inhibition using a GAT1 inhibitor, NO711 (40 μM). Tonic holding currents showed larger amplitudes after bath application of NO711 ($I_{NO711}$) than before ($I_{tonic}$) in all evaluated cells. Although the increase in tonic currents induced by NO711 ($\Delta I_{NO711}$) was larger in *Ube3a*$^{m-/p+}$ mice than in wild-type mice, $I_{tonic}$ itself was significantly decreased ($P < 0.001$; Fig. 2, C and D). Consequently, $I_{NO711}$ was not different between *Ube3a*$^{m-/p+}$ and wild-type mice ($P = 0.51$; Fig. 2D), suggesting that excessive uptake of GABA via GAT1 could give rise to decreased tonic inhibition in *Ube3a*$^{m-/p+}$ mice. Indeed, GAT1 protein concentrations in the cerebellum of *Ube3a*$^{m-/p+}$ mice were significantly elevated at P32 ($P < 0.05$; Fig. 3, A and B), and a tendency toward an elevation was seen in 5-month-old mice (fig. S4). In contrast, expression of $GABA_A$ receptor subunit α6 did not differ between wild-type and *Ube3a*$^{m-/p+}$ mice (Fig. 3, A and B).

### Ube3a binds to GAT1 and regulates its stability

Because GAT1 mRNA expression did not increase in *Ube3a*$^{m-/p+}$ mice [GAT1/GAPDH (glyceraldehyde-3-phosphate dehydrogenase): wild-type, 1.00 ± 0.22, $n$ = 3, versus *Ube3a*$^{m-/p+}$, 1.13 ± 0.28, $n$ = 3; $P$ = 0.65], aberrant posttranscriptional modifications relevant to Ube3a deficiency seemed a likely mechanism for increased GAT1 activity. To test this, we performed an in vitro degradation assay (*25*, *26*) using cerebellar lysates and found that GAT1 protein rapidly degraded in cerebellar lysates derived from wild-type mice, but was stable in those derived from *Ube3a*$^{m-/p+}$ mice (Fig. 3, C and D). This suggests that Ube3a may be involved in degradation of GAT1 in the mouse cerebellum.

We next investigated whether GAT1 interacts with Ube3a in intact cells. Human embryonic kidney (HEK) 293 cells were transfected with or without FLAG-GAT1 and/or Myc-Ube3a. Myc-Ube3a was immunoprecipitated with anti-Myc antibody from whole-cell lysates after immunoblotting with anti-FLAG antibody. FLAG-GAT1 was coprecipitated with Myc-Ube3a (Fig. 3E, middle and bottom panels, lane 1 versus lane 2). Alternatively, FLAG-GAT1 was immunoprecipitated with anti-FLAG antibody from whole-cell lysates after immunoblotting with anti-Myc antibody. Myc-Ube3a was coprecipitated with FLAG-GAT1 (Fig. 3E, top panel, lane 4). GAT1 binding to Myc-Ube3a was detected as indicated by the arrow in Fig. 3E (middle and bottom panels, lane 2). Simultaneously, immunoblot analysis with anti-FLAG or anti-GAT1 confirmed oligomerized GAT1 protein, which was detected as a smear. Our results are consistent with those of previous reports that exogenously overexpressed GAT1 protein tends to be oligomerized in cultured cells (*27*, *28*). Because denaturing gels were used, these results do not directly show that Ube3a binds to monomeric GAT1 in intact cells but do suggest a potential interaction between Ube3a and GAT1.

To investigate whether endogenous Ube3a can bind to GAT1 in mouse cerebellum, we performed immunoprecipitation after immunoblotting

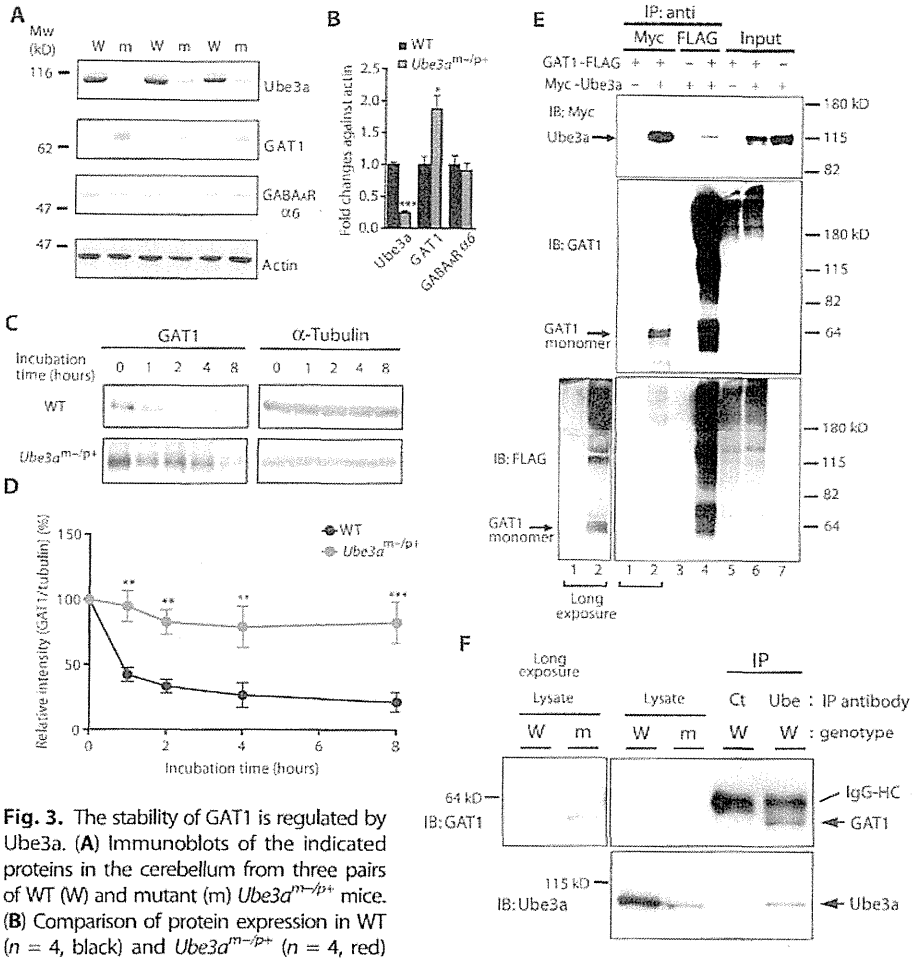


**Fig. 3.** The stability of GAT1 is regulated by Ube3a. (**A**) Immunoblots of the indicated proteins in the cerebellum from three pairs of WT (W) and mutant (m) *Ube3a*$^{m-/p+}$ mice. (**B**) Comparison of protein expression in WT ($n$ = 4, black) and *Ube3a*$^{m-/p+}$ ($n$ = 4, red) mice. $^{*}P < 0.05$, $^{***}P < 0.001$, unpaired $t$ test. (**C**) Representative immunoblots of an in vitro degradation assay for GAT1. (**D**) Percentage of GAT1 remaining after the indicated incubation times in WT ($n$ = 4, black) and *Ube3a*$^{m-/p+}$ ($n$ = 4, red) mice. The percentage of GAT1 protein was normalized to α-tubulin and calculated as the mean ± SEM from four mice. $^{**}P < 0.01$, $^{***}P < 0.001$ by post hoc analysis for the genotypic group comparison after a two-way repeated-measures analysis of variance (ANOVA). (**E**) Interaction between GAT1 and Ube3a in HEK293 cells transfected with or without FLAG-GAT1 and/or Myc-Ube3a. (**F**) Interaction of endogenous GAT1 and Ube3a in the mouse cerebellum. Ube3a protein was immunoprecipitated (IP) with anti-Ube3a (Ube) or control immunoglobulin G (IgG) (Ct) antibody from lysates prepared from WT mouse cerebellum. Then, the immunoprecipitates and the original cell lysates prepared from WT and mutant *Ube3a*$^{m-/p+}$ mice were separated by SDS–polyacrylamide gel electrophoresis (SDS-PAGE), followed by immunoblotting (IB) with either anti-GAT1 or anti-Ube3a antibody. HC, heavy chain.

assays using lysates prepared with immunoprecipitation lysis buffer containing the proteasome inhibitor MG132 from wild-type mouse cerebellum (see Supplementary Materials and Methods). As shown in Fig. 3F, endogenous GAT1 was detected in the immunoprecipitate with anti-Ube3a antibody, but not with control IgG. This result indicates that endogenous Ube3a binds to endogenous GAT1 in mouse cerebellum.

### Electrophysiological cerebellar dysfunction in *Ube3a*$^{m-/p+}$ mice in vitro is due to decreased tonic inhibition

Tonic $GABA_A$ receptor–mediated conductance can control the excitability of cerebellar granule cells by decreasing total membrane input resistance (*29*–*31*), a phenomenon referred to as shunting inhibition. However, other membrane conductances such as leak $K^+$ currents (*32*) may compensate for persistently low input resistance. To determine whether cerebellar granule cell excitability is altered by the decreased tonic inhibition observed in *Ube3a*$^{m-/p+}$ mice, we evaluated resting and firing membrane properties using whole-cell current-clamp recordings. Cerebellar granule cells of *Ube3a*$^{m-/p+}$ mice showed higher input resistance (table S1) and required lower current injection to reach action potential threshold (Fig. 4A and table S1). The relationship between firing rate and the injected current shifted to the left until the injected currents reached about 20 pA, indicating that lower current injections resulted in higher firing rates in *Ube3a*$^{m-/p+}$ mice (Fig. 4B). In contrast, the current-voltage relationships for the leak conductances and input resistances in the presence of BIC, strychnine, 6-cyano-7-nitroquinoxaline-2,3-dione (CNQX), D-(−)-2-amino-5-phosphonovaleric acid (AP5), and tetrodotoxin (TTX) were not significantly different (leak conductance: $P = 0.98$, Kolmogorov-Smirnov test, Fig. 4C; input resistance: $P = 0.82$, unpaired $t$ test, table S1), indicating a lack of adaptive regulation for neuronal excitability. Bath application of low-dose 4,5,6,7-tetrahydroisothiazolo-[5,4-c]pyridin-3-ol (THIP; 500 nM), a selective agonist for extrasynaptic $GABA_A$ receptors containing the δ subunit (*33*), significantly increased tonic holding currents (from 0.84 ± 0.35 to 4.26 ± 0.6 pA/pF; $P < 0.01$, paired $t$ test; $n = 4$) and reduced the excitability (Fig. 4D and fig. S5D) of *Ube3a*$^{m-/p+}$ cerebellar granule cells. THIP (500 nM) also increased the tonic holding currents and tempered the excitability in wild-type mice, but the efficacy was lower than that in *Ube3a*$^{m-/p+}$ mice (fig. S5). These findings demonstrate that the membrane excitability of cerebellar granule cells increased to near action potential threshold due to the decreased tonic inhibition in *Ube3a*$^{m-/p+}$ mice.

We also found that cerebellar granule cells of *Ube3a*$^{m-/p+}$ mice exhibited spike rate adaptation (Fig. 4, A and B) corresponding to the decreased after-hyperpolarization (table S1). The spike rate adaptation was still observed in the presence of THIP (Fig. 4D). The half width and rise time of action potentials were also increased in cerebellar granule cells of *Ube3a*$^{m-/p+}$ mice (table S1). Together, these results suggest that intrinsic firing properties are altered by Ube3a deficiency in cerebellar granule cells.

Purkinje cells are the only output cells in the cerebellar cortex. To determine whether the decreased tonic inhibition in cerebellar granule cells could be attributed to cerebellar dysfunction, we next evaluated the spontaneous firing properties of Purkinje cells in acutely prepared

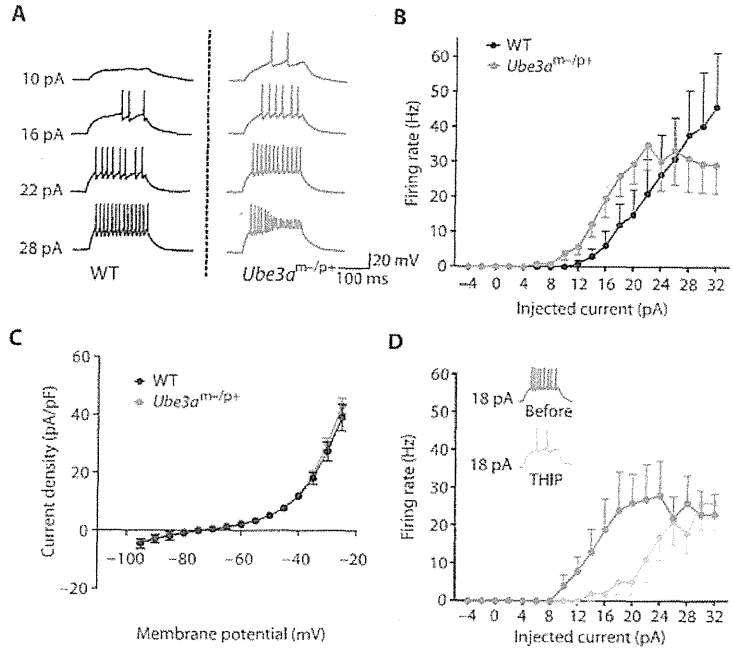


**Fig. 4.** Decreased tonic inhibition increases cerebellar granule cell membrane excitability in *Ube3a*$^{m-/p+}$ mice. (**A**) Representative responses of cerebellar granule cells (voltage held at −65 mV) to current injection in WT and *Ube3a*$^{m-/p+}$ mice. (**B**) Averaged input-output relationship of cerebellar granule cells from WT ($n$ = 10) and *Ube3a*$^{m-/p+}$ ($n$ = 12) mice. (**C**) Averaged current-voltage relationship for leak $K^+$ conductance in cerebellar granule cells from WT ($n$ = 10) and *Ube3a*$^{m-/p+}$ ($n$ = 10) mice. (**D**) Averaged input-output relationship in cerebellar granule cells ($n$ = 5) from *Ube3a*$^{m-/p+}$ mice in the absence (red trace) or presence of THIP (blue trace). Inset traces show representative responses of cerebellar granule cells (voltage held at −65 mV) to 18-pA current injection in the absence (red) or presence of THIP (blue). All data are means ± SEM.

cerebellar brain slices with extracellular single-unit recordings. With the exception of three Purkinje cells in *Ube3a*$^{m-/p+}$ mice that showed a characteristic tonic silent pattern, all successfully recorded Purkinje cells from wild-type and *Ube3a*$^{m-/p+}$ mice showed either tonic or trimodal (*34*) firing patterns (Fig. 5A). Although only half of the wild-type Purkinje cells presented a tonic pattern [as shown in previous reports (*34*, *35*)], the proportion reached 80% in *Ube3a*$^{m-/p+}$ Purkinje cells (Fig. 5B), with only 2 of 25 cells displaying the trimodal pattern. The firing pattern was consistent in each cell throughout recordings lasting over 5 min. However, bath application of THIP (500 nM) altered the firing pattern from tonic to trimodal in four of five Purkinje cells in *Ube3a*$^{m-/p+}$ mice (Fig. 5C). The same change was observed in the tonic firing pattern in wild-type mice (two of two cells; fig. S6A), but the trimodal pattern in wild-type mice was not altered by THIP (two of two cells; fig. S6B). It has been shown that intrinsic Purkinje cell firing patterns show a trimodal pattern, because blockage of excitatory and inhibitory inputs changed the firing pattern from tonic to trimodal (*34*). THIP increased tonic holding currents in cerebellar granule cells (see above) but not in Purkinje cells from *Ube3a*$^{m-/p+}$ mice (Fig. 5D). Thus, decreased tonic inhibition leads to increases in spontaneous synaptic inputs from cerebellar granule cells to Purkinje cells and can account for the abnormally high proportion of Purkinje cells displaying tonic firing patterns in *Ube3a*$^{m-/p+}$ mice.

The Purkinje cell firing rate and the coefficient of variance of the interspike intervals during tonic firing did not differ between wild-type and *Ube3a*$^{m-/p+}$ mice (fig. S7). However, Ube3a deficiency could affect the intrinsic firing properties of Purkinje cells as witnessed by the characteristic tonic silent pattern that was not affected by THIP ($n$ = 2).

### THIP can partially rescue the cerebellar dysfunction in vivo

Previous studies have reported that hind paw width and stride in *Ube3a*$^{m-/p+}$ mice were larger than (*36*, *37*) or similar to those in wild-type mice (*2*). In our evaluation, they were not significantly different ($P$ = 0.44 and 0.73, respectively; Fig. 6, A and B). However, gait analysis revealed that the angle between the left and right hind paw axes (paw abduction) was significantly larger in *Ube3a*$^{m-/p+}$ mice ($P$ < 0.001; Fig. 6, A and B). To discern the contribution of decreased $I_{tonic}$ to cerebellar ataxia, we evaluated the effects of THIP in vivo in mice aged 3 to 5 months. Intraperitoneal injection of THIP (2.5 mg/kg) reduced the hind paw abduction in *Ube3a*$^{m-/p+}$ mice without affecting the width or stride (Fig. 6, C to E). In contrast, THIP (2.5 mg/kg) did not alter gait parameters in wild-type mice (fig. S8, A and B).

When mice were held by their tails (tail suspension test), *Ube3a*$^{m-/p+}$ mice (*37*) as well as mice of other strains presenting cerebellar ataxia (*23*, *38*) show a clasping reflex, represented by forelimb clasping and flexion to the body. We evaluated the clasping behavior with a previously reported scoring method (*38*) and by measuring the forelimb angle against the body axis viewed laterally. Scoring was conducted blindly, with evaluators unaware of the mouse genotypes or the drugs used. All *Ube3a*$^{m-/p+}$ mice showed a mild to moderate clasping reflex (fig. S9A) and smaller forelimb angles compared with wild-type mice due to forelimb flexion (Fig. 6, F and G). Five of seven *Ube3a*$^{m-/p+}$ mice showed improved clasping reflexes after treatment with THIP (2.5 mg/kg) intraperitoneally (fig. S9B). THIP also significantly increased the forelimb angles in *Ube3a*$^{m-/p+}$ mice ($P$ < 0.01; Fig. 6, H and I, and movie S1) but not in wild-type mice ($P$ = 0.56; fig. S8C).

Consistent with previous findings, time spent on an accelerating rotarod was shorter in *Ube3a*$^{m-/p+}$ mice than in wild-type mice (Fig. 7A). This was improved significantly by THIP at 1.25 mg/kg ($P$ < 0.05) but not significantly by THIP at 2.5 mg/kg ($P$ = 0.20; Fig. 7B). Comparison of this effect between wild-type and *Ube3a*$^{m-/p+}$ mice revealed that THIP (1.25 mg/kg) was specifically effective for *Ube3a*$^{m-/p+}$ mice but not for wild-type mice (Fig. 7C and fig. S8D).

THIP concentrations in the rat brain have been reported to reach up to 700 nM with a subcutaneous administration of 2.5 mg/kg (*39*), a concentration much lower than that needed to activate nonspecific $GABA_A$ receptors that lack the δ subunit (*33*). Therefore, these in vivo analyses demonstrate that decreased tonic inhibition in cerebellar granule cells underlies the cerebellar dysfunction in *Ube3a*$^{m-/p+}$ mice.

## DISCUSSION

Here, we have demonstrated that cerebellar granule cells in a mouse model of Angelman syndrome exhibit decreased tonic inhibition and aberrant membrane excitability. Pharmacological enhancement of

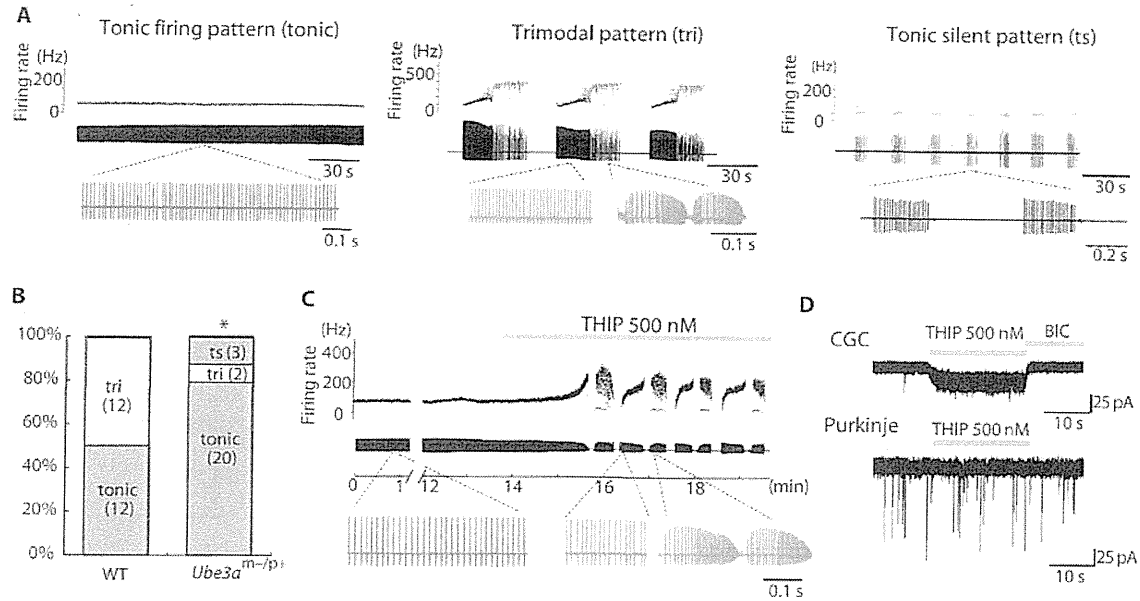


**Fig. 5.** Administration of THIP alters Purkinje cell firing patterns in *Ube3a*$^{m-/p+}$ mice. (**A**) Three representative firing patterns observed in Purkinje cells using single-unit recordings. Firing rates (upper traces), waveforms (middle traces), and expanded waveforms (bottom traces) are plotted. Left panel: continuous, stable firing rate [tonic pattern (tonic)]; middle panel: recurrence of tonic and burst-like firing interspersed with silent periods [trimodal pattern (tri)]; right panel: short, stable firing interrupted by repetitive pause and followed by a silent period [tonic silent pattern (ts)]. (**B**) Proportion of each firing pattern in WT ($n$ = 24) and *Ube3a*$^{m-/p+}$ ($n$ = 25) mice. The number of cells is indicated in each column. The tonic-pattern ratio was compared between WT and *Ube3a*$^{m-/p+}$ mice with a $\chi^2$ test. *$P$ < 0.05. (**C**) Representative traces illustrating the change in firing pattern caused by bath application of THIP (500 nM) in a brain slice from a *Ube3a*$^{m-/p+}$ mouse. (**D**) Representative current traces of cerebellar granule cells (CGC) and Purkinje cells from *Ube3a*$^{m-/p+}$ mice showing the effect of focal THIP (500 nM) application on base holding currents. All data are means ± SEM.

tonic inhibition reduces motor dysfunction in these mice, suggesting that decreased tonic inhibition is an important mechanism underlying the movement disorder in Angelman syndrome. Furthermore, we have shown that Ube3a deficiency reduces the degradation of GAT1, and that this, in turn, decreases tonic inhibition.

Extrasynaptic $GABA_A$ receptor–mediated tonic inhibition was first identified in rat cerebellar granule cells (*40*), and its pharmacological manipulation has been shown to regulate cerebellar granule cell (*29*–*31*) and Purkinje cell (*30*) excitability. However, the effects of long-term deficiencies in tonic inhibition on cerebellar function have not been fully understood because extrasynaptic $GABA_A$ receptor–null mutant mice did not show ataxia as a result of compensatory increases in potassium conductance in cerebellar granule cells (*32*). We have shown that decreased $I_{tonic}$ resulting from the reduction in ambient GABA concentrations causes cerebellar dysfunction in *Ube3a*$^{m-/p+}$ mice. Because cerebellar ataxia was successfully improved by administration of an extrasynaptic $GABA_A$ receptor–selective agonist, THIP, our results highlight the importance of ambient GABA regulation in maintaining cerebellar function by regulating $I_{tonic}$ and cerebellar granule cell excitability.

More specifically, we have discovered that Ube3a regulates tonic inhibition by controlling the degradation of GAT1. Although GAT1 can be expressed in astrocytes as well as neurons (*22*), Ube3a is expressed exclusively in neurons (*18*, *24*). Therefore, our findings suggest the importance of neuronal GAT1 in the regulation of ambient GABA concentrations in the cerebellar granule cell layer. Neuronal GAT1 may also affect sIPSCs by decreasing decay time (*23*); however, our evidence showing that sIPSCs were not altered in cerebellar granule cells from *Ube3a*$^{m-/p+}$ mice is in agreement with previous data (*20*). Given that inhibitory input onto cerebellar granule cells shifts from phasic to tonic along with development (*19*), it is conceivable that the dominant effect of GAT1 is exclusively on tonic inhibition.

Our in vivo studies using THIP represent a potential therapeutic strategy for Angelman syndrome by compensating for the decreased tonic inhibition. Tiagabine, an antiepileptic drug that inhibits GAT1, might also be effective for similar reasons. However, for the clinical administration of these drugs, the range of therapeutic doses should be considered carefully because excessive tonic inhibition can also induce neuronal dysfunction (*16*, *17*). The regulatory mechanisms for ambient GABA in the brain differ from region to region. For example, GAT1 in the rat thalamus is exclusively expressed in astrocytes (*41*), which implies unchanged tonic inhibition in the thalamus of Angelman syndrome individuals. Therefore, a therapeutic increase in tonic inhibition may adversely affect the functions of the thalamo-cortical network. This implication is supported by a clinical report of vigabatrin-induced seizure aggravation in Angelman syndrome (*42*). Whereas THIP (2.5 mg/kg) did not affect rotarod performance in wild-type mice in line with the findings of a previous report (*43*), a recent study reported reduced locomotor activity in wild-type mice after administration of THIP (2.0 mg/kg) (*44*). Thus, possible adverse effects of THIP (2.5 mg/kg) could mask improvements in cerebellar ataxia in *Ube3a*$^{m-/p+}$ mice, resulting in unchanged rotarod performance with the higher dose of THIP. Whereas tiagabine shows higher affinity in the thalamus than the cerebellar granule cell layer (*45*), THIP displays the opposite pattern (*46*). Thus, we propose that low doses of THIP potentially may be an effective treatment for the cerebellar ataxia in Angelman syndrome.

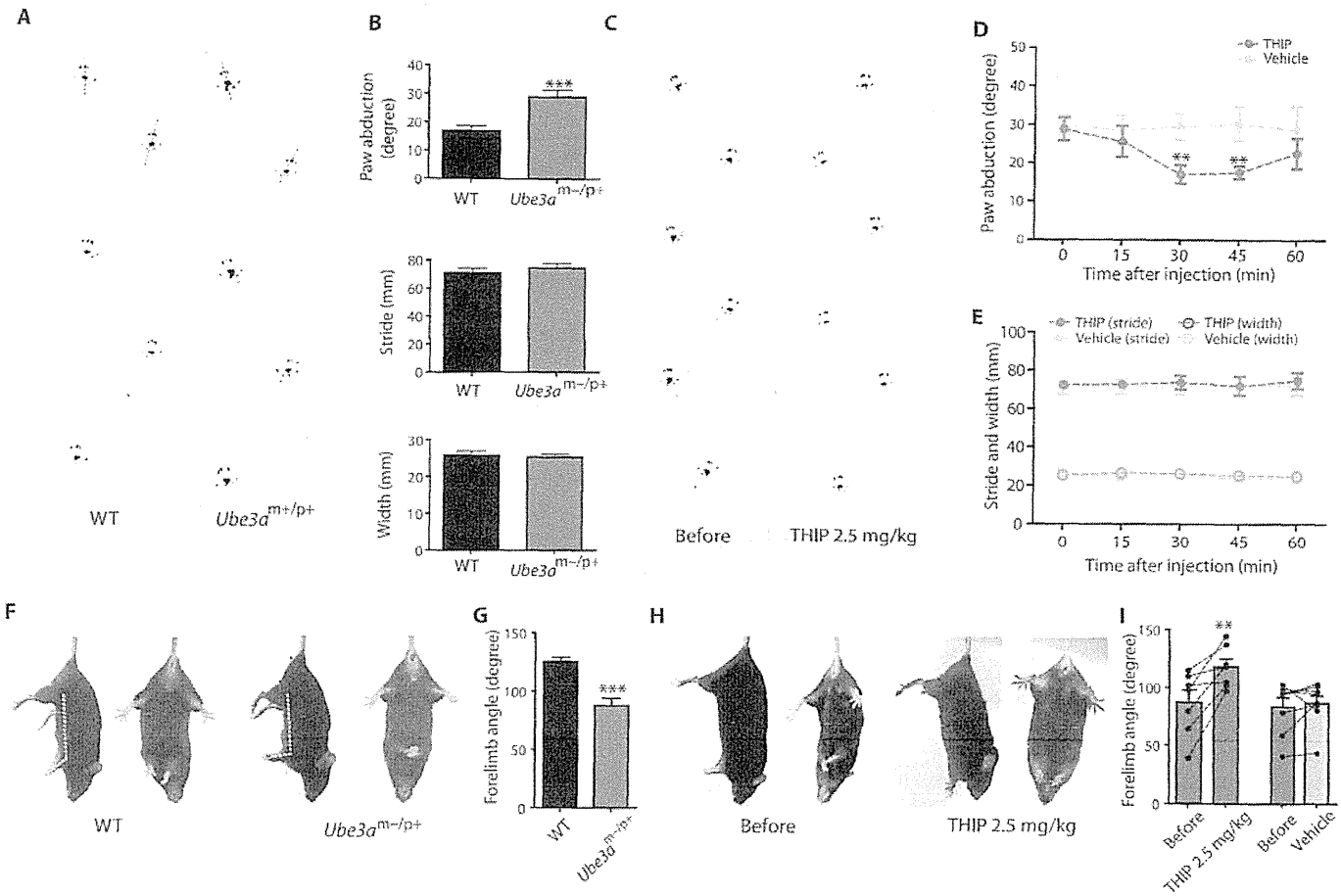


**Fig. 6.** Administration of THIP improves ataxia in *Ube3a*$^{m-/p+}$ mice. (**A** and **B**) Representative footprint traces (A) and comparison of each parameter (B) in WT ($n$ = 10) and *Ube3a*$^{m-/p+}$ ($n$ = 11) mice. (**C**) Representative footprint traces before and 30 min after administration of THIP (2.5 mg/kg) in *Ube3a*$^{m-/p+}$ mice. (**D**) Changes over time of paw abduction angles after injection of THIP (blue) or saline (gray) in *Ube3a*$^{m-/p+}$ mice. (**E**) Analyses over time of stride length (filled circles) and base width (empty circles) after administering THIP (blue) or saline (gray) in *Ube3a*$^{m-/p+}$ mice. (**F**) Representative limb postures responding to tail suspension in WT and *Ube3a*$^{m-/p+}$ mice. (**G**) Comparison of the forelimb angles against body axes in the tail suspension test. Angles were evaluated from a side view as indicated by dotted lines in (F) (WT, $n$ = 14; *Ube3a*$^{m-/p+}$, $n$ = 15). (**H**) Representative responses to tail suspension before and 40 min after THIP (2.5 mg/kg) administration. (**I**) Effects of THIP and saline on forelimb angles in the tail suspension test. $^{**}P < 0.01$, $^{***}P < 0.001$. Unpaired $t$ test (B and G), one-way repeated-measures ANOVA (D and E), or paired $t$ tests (I) were performed. Data are means ± SEM.

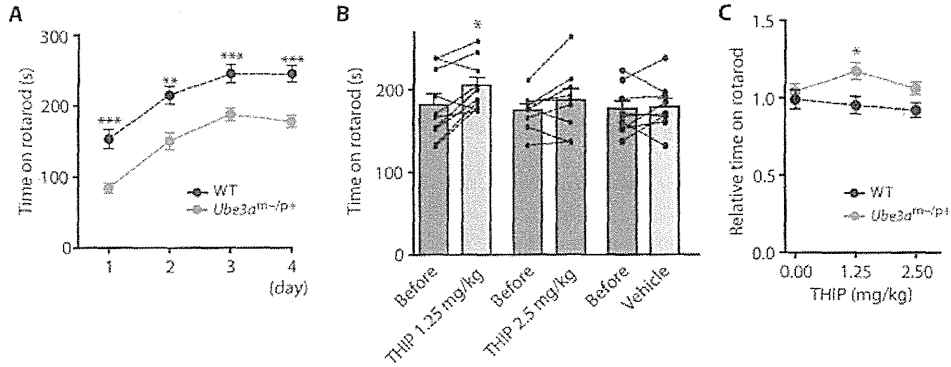


**Fig. 7.** Administration of THIP improves rotarod scores in *Ube3a*$^{m-/p+}$ mice. (**A**) Comparison of time spent on a rotarod between WT (black) and *Ube3a*$^{m-/p+}$ (red) mice. (**B**) Effects of THIP (1.25 or 2.5 mg/kg) or saline on time spent on a rotarod in *Ube3a*$^{m-/p+}$ mice. (**C**) Comparison of the dose-dependent effects of THIP on time spent on a rotarod in WT (black) and *Ube3a*$^{m-/p+}$ (red) mice. The amount of time 30 min after an injection was normalized to the time before the injection. $^{*}P < 0.05$, $^{**}P < 0.01$, $^{***}P < 0.001$. Two-way repeated-measures ANOVA (A and C) or paired $t$ tests (B) were performed. Data are means ± SEM.

Partial rescue by in vivo THIP administration in *Ube3a*$^{m-/p+}$ mice suggests that other mechanisms, such as dysfunction of the nigrostriatal pathway (*37*), could be involved in the motor dysfunction in Angelman syndrome. We also observed THIP-insensitive aberrant firing properties in both cerebellar granule cells and Purkinje cells from *Ube3a*$^{m-/p+}$ mice, the mechanisms of which are still being elucidated. Increased Na/K-ATPase (adenosine triphosphatase) and lower resting membrane potentials were recently shown in CA1 hippocampal neurons from *Ube3a*$^{m-/p+}$ mice (*47*). The same deregulation might explain the tonic-silent pattern of Purkinje cell firing in *Ube3a*$^{m-/p+}$ mice.

The spike rate adaptation with lower amplitude after hyperpolarization of cerebellar granule cells might result from deactivation of large-conductance $K^+$ (BK) channels (*48*) due to the decreased activity of calcium/calmodulin-dependent protein kinase II in *Ube3a*$^{m-/p+}$ mice (*5*). Previous in vivo analysis in *Ube3a*$^{m-/p+}$ mice showed that aberrant Purkinje cell firing consisted of the increased frequency and rhythmicity of simple spikes (*49*). Because simple spikes are modulated by parallel fiber input, our observation of lower threshold currents for eliciting action potentials and reduced repetitive firing in cerebellar granule cells in vitro can explain the results of in vivo Purkinje cell firing analysis. Decreased burst firing of cerebellar granule cells due to reduced repetitive firing can cause the higher rhythmicity of simple spikes. Because reduced ongoing firing due to $I_{tonic}$ and intrinsic bursting properties are both critical for shaping a high signal-to-noise ratio of information flow via cerebellar granule cells in vivo (*31*), the collapse of this regulation might synergistically aggregate cerebellar dysfunction in *Ube3a*$^{m-/p+}$ mice.

Because neuronal GAT1 is widely expressed in the CNS, its attenuated degradation could contribute to other symptoms of Angelman syndrome (*4*) and to the phenotype-genotype correlation relevant to the hemizygosity of $GABA_A$ receptor subunit genes such as α5 and β3 (*11*, *12*). Although the number of $GABA_A$ benzodiazepine-binding receptors did not decrease (*50*), the relative expression of β3 and α5 was reduced in Angelman syndrome patients lacking these genes (*51*). Because β3 is a major component of extrasynaptic $GABA_A$ receptors (*15*) and α5 is primarily expressed extrasynaptically in the hippocampus (*52*), tonic inhibition may be lower in these Angelman syndrome patients in conjunction with Ube3a deficiency.

Here, we have shown that the GABAergic dysfunction in Ube3a deficiency is caused by attenuated degradation of GAT1. The ubiquitin-proteasome degradation pathway has been recently implicated as a key regulator of neuronal activity by controlling the membrane trafficking and stability of receptor channels (*53*, *54*) and transporters (*55*). To the best of our knowledge, a specific E3 ligase and its target proteins have not been determined in inhibitory systems. Given that GAT1 and Ube3a expression increases during neurodevelopment (*56*, *57*), this study provides new insight into the synaptic plasticity of inhibitory neural systems and their pathophysiological contribution to neurodevelopmental disorders.

## MATERIALS AND METHODS

### Animals

All experiments conformed to the guidelines for the ethical use of animals for experimentation issued by Hamamatsu University School of Medicine. *Ube3a*-null mutant mice were generated on a C57BL/6 genetic background at Nagasaki University (*8*) and shipped to Hamamatsu University School of Medicine for all experimental procedures. A heterogeneous female mouse lacking a paternal *Ube3a* gene was crossed with a wild-type male mouse to obtain either heterogeneous mice lacking the maternal *Ube3a* gene (*Ube3a*$^{m-/p+}$) or littermate wild-type mice. Genotyping was carried out by polymerase chain reaction (PCR) of mouse tail DNA as described previously (*8*).

### Electrophysiology

Unless otherwise noted, we carried out all electrophysiological analyses in P25 to P28 *Ube3a*$^{m-/p+}$ or littermate wild-type mice. Recordings from mice of each genotype were performed on consecutive days whenever possible. Recording temperature was set at 35°C except for the initial series of recordings for tonic currents at P25 to P28 or P75 to P82, which were recorded at room temperature. We evaluated the tonic currents by focal application of BIC (20 μM). For the first series of experiments (Fig. 1A, C and D), we also evaluated the tonic current by application of SR95531 (10 μM). Because the results obtained using BIC and SR95531 were not different (fig. S10), consistent with the findings of a previous report (*58*), we pooled both groups of data for further analyses. Detailed protocols are available in Supplementary Materials and Methods.

### Immunoblotting

Mouse (P28 to P33) cerebellum samples were homogenized and lysed in lysis buffer. Blots were probed with antibodies and detected using horseradish peroxidase–conjugated secondary antibody and an enhanced luminescence kit (GE Healthcare). The experimental details and a list of antibodies are provided in Supplementary Materials and Methods.

### Real-time PCR

Total RNAs obtained from mouse (P28 to P33) cerebellar samples were extracted with TRIzol reagent (Invitrogen). Complementary DNAs (cDNAs) were synthesized and quantitative real-time PCR was performed to validate the expression changes of selected genes in accordance with the manufacturer's protocols. Real-time PCRs were carried out in triplicate for each sample. Details are shown in Supplementary Materials and Methods.

### Analysis of the interaction between Ube3a and GAT1

HEK293 cells were maintained in Dulbecco's modified Eagle's medium supplemented with 10% fetal bovine serum. cDNAs encoding mouse GAT1 (*59*) (provided by H. A. Lester, California Institute of Technology) were cloned into pCMV-3Tag-8 (Invitrogen). The pcDNA3-Myc3-E6AP (Ube3a) expression plasmid was provided by T. Ohta (St. Marianna University School of Medicine). Plasmids were transfected into HEK293 cells with the calcium phosphate method. For immunoprecipitation, cell lysates were incubated with 2 μg of antibodies and protein G+ Sepharose 4FF (GE Healthcare) at 4°C for 1 hour as previously described (*26*). Immunocomplexes were washed five times with lysis buffer. Immunoprecipitated samples as well as the original cell lysates (input) were separated by 7% SDS-PAGE and transferred from the gel onto a polyvinylidene difluoride membrane (Millipore), followed by immunoblotting. Proteins were visualized with an enhanced chemiluminescence system (Perkin Elmer). Details of the methods of endogenous protein analysis are provided in Supplementary Materials and Methods.

### In vitro degradation assay

Mouse (P28 to P33) cerebellum samples were extracted with lysis buffer as described above. Cerebellum lysate (100 μg) was incubated in 20 μl of ubiquitination mixture [50 mM tris-HCl (pH 8.3), 5 mM $MgCl_2$, 2 mM dithiothreitol, 5 mM adenosine 5′-triphosphate, and ubiquitin (1 mg/ml)] for 0, 1, 2, 4, or 8 hours at 37°C. After incubation, each sample was subjected to 8% SDS-PAGE, followed by immunoblot analysis with anti-GAT1 antibody (Abcam) or α-tubulin antibody (Sigma). Details can be found in previous reports (*60*).

### In vivo analysis of motor functions

All in vivo analyses were performed with male or female mice aged 3 to 5 months. For the footprint analysis and the tail suspension test, evaluators were unaware of either the genotype or the injected drug until analyses were completed. Except for the footprint analysis, the effect of THIP was evaluated 30 to 45 min after intraperitoneal administration. For the footprint analysis, hind paws were painted with black ink. Mice were then allowed to walk in a narrow corridor placed on white paper. We averaged the measurements from three trials for each recording. For the tail suspension test, mice were suspended by the tail; after stabilization, the clasping reflex was evaluated according to previously described scoring scales (*38*). Upper limb angles against body axes were evaluated by photographic capture of limb positions from a lateral view. For accelerating rotarod analysis, the rotational speed increased from 5 to 50 rpm over a period of 5 min. Three trials were performed for each recording, and median values were used for statistical analyses. Details are provided in Supplementary Materials and Methods.

### Statistical analyses

Unless otherwise noted, statistical analyses were performed with unpaired Student's *t* tests. ANOVA (one- or two-way) and Bonferroni post hoc analysis were used to analyze multiple comparisons. Two-group comparisons were made with Student's *t* tests, except for the cases of sIPSC frequency and Purkinje cell firing properties. These were analyzed with Mann-Whitney *U* tests. Data are presented as means ± SEM, and $P < 0.05$ was considered to represent statistical significance.

## SUPPLEMENTARY MATERIALS

www.sciencetranslationalmedicine.org/cgi/content/full/4/163/163ra157/DC1

Materials and Methods

Fig. S1. Ubiquitous expression of maternally expressed Ube3a in the cerebellar cortex.

Fig. S2. Electron micrographs of the cerebellar granule layer in wild-type and *Ube3a*$^{m-/p+}$ mice.

Fig. S3. Unaltered sIPSCs of cerebellar granule cells from *Ube3a*$^{m-/p+}$ mice.

Fig. S4. Accumulation of GAT1 protein in 5-month-old *Ube3a*$^{m-/p+}$ mouse cerebellum.

Fig. S5. Effects of THIP on cerebellar granule cell membrane excitability in wild-type and *Ube3a*$^{m-/p+}$ mice.

Fig. S6. Effects of THIP on Purkinje cell firing patterns in wild-type mice.

Fig. S7. Firing properties of Purkinje cells that display tonic firing.

Fig. S8. Effects of THIP administration on motor functions in wild-type mice.

Fig. S9. Scoring for the clasping reflex during the tail suspension test.

Fig. S10. Comparison of tonic currents after treatments with BIC and SR95531.

Table S1. Resting membrane and firing properties of cerebellar granule cells from wild-type and *Ube3a*$^{m-/p+}$ mice.

Table S2. Primers for PCR.

Movie S1. Tail suspension test.

## REFERENCES AND NOTES

1. U. Albrecht, J. S. Sutcliffe, B. M. Cattanach, C. V. Beechey, D. Armstrong, G. Eichele, A. L. Beaudet, Imprinted expression of the murine Angelman syndrome gene, *Ube3a*, in hippocampal and Purkinje neurons. *Nat. Genet.* **17**, 75–78 (1997).
2. Y. H. Jiang, D. Armstrong, U. Albrecht, C. M. Atkins, J. L. Noebels, G. Eichele, J. D. Sweatt, A. L. Beaudet, Mutation of the Angelman ubiquitin ligase in mice causes increased cytoplasmic p53 and deficits of contextual learning and long-term potentiation. *Neuron* **21**, 799–811 (1998).
3. T. Kishino, M. Lalande, J. Wagstaff, UBE3A/E6-AP mutations cause Angelman syndrome. *Nat. Genet.* **15**, 70–73 (1997).
4. C. A. Williams, H. Angelman, J. Clayton-Smith, D. J. Driscoll, J. E. Hendrickson, J. H. Knoll, R. E. Magenis, A. Schinzel, J. Wagstaff, E. M. Whidden, R. T. Zori, Angelman syndrome: Consensus for diagnostic criteria. Angelman Syndrome Foundation. *Am. J. Med. Genet.* **56**, 237–238 (1995).
5. E. J. Weeber, Y. H. Jiang, Y. Elgersma, A. W. Varga, Y. Carrasquillo, S. E. Brown, J. M. Christian, B. Mirnikjoo, A. Silva, A. L. Beaudet, J. D. Sweatt, Derangements of hippocampal calcium/calmodulin-dependent protein kinase II in a mouse model for Angelman mental retardation syndrome. *J. Neurosci.* **23**, 2634–2644 (2003).
6. K. Yashiro, T. T. Riday, K. H. Condon, A. C. Roberts, D. R. Bernardo, R. Prakash, R. J. Weinberg, M. D. Ehlers, B. D. Philpot, Ube3a is required for experience-dependent maturation of the neocortex. *Nat. Neurosci.* **12**, 777–783 (2009).
7. P. L. Greer, R. Hanayama, B. L. Bloodgood, A. R. Mardinly, D. M. Lipton, S. W. Flavell, T. K. Kim, E. C. Griffith, Z. Waldon, R. Maehr, H. L. Ploegh, S. Chowdhury, P. F. Worley, J. Steen, M. E. Greenberg, The Angelman Syndrome protein Ube3A regulates synapse development by ubiquitinating arc. *Cell* **140**, 704–716 (2010).
8. K. Miura, T. Kishino, E. Li, H. Webber, P. Dikkes, G. L. Holmes, J. Wagstaff, Neurobehavioral and electroencephalographic abnormalities in *Ube3a* maternal-deficient mice. *Neurobiol. Dis.* **9**, 149–159 (2002).
9. B. Dan, S. G. Boyd, Angelman syndrome reviewed from a neurophysiological perspective. The *UBE3A-GABRB3* hypothesis. *Neuropediatrics* **34**, 169–176 (2003).
10. J. J. Yi, M. D. Ehlers, Emerging roles for ubiquitin and protein degradation in neuronal function. *Pharmacol. Rev.* **59**, 14–39 (2007).
11. A. C. Lossie, M. M. Whitney, D. Amidon, H. J. Dong, P. Chen, D. Theriaque, A. Hutson, R. D. Nicholls, R. T. Zori, C. A. Williams, D. J. Driscoll, Distinct phenotypes distinguish the molecular classes of Angelman syndrome. *J. Med. Genet.* **38**, 834–845 (2001).
12. K. Egawa, N. Asahina, H. Shiraishi, K. Kamada, F. Takeuchi, S. Nakane, A. Sudo, S. Kohsaka, S. Saitoh, Aberrant somatosensory-evoked responses imply GABAergic dysfunction in Angelman syndrome. *Neuroimage* **39**, 593–599 (2008).
13. I. Mody, R. A. Pearce, Diversity of inhibitory neurotransmission through $GABA_A$ receptors. *Trends Neurosci.* **27**, 569–575 (2004).
14. M. Farrant, Z. Nusser, Variations on an inhibitory theme: Phasic and tonic activation of $GABA_A$ receptors. *Nat. Rev. Neurosci.* **6**, 215–229 (2005).
15. Z. Nusser, W. Sieghart, P. Somogyi, Segregation of different $GABA_A$ receptors to synaptic and extrasynaptic membranes of cerebellar granule cells. *J. Neurosci.* **18**, 1693–1703 (1998).
16. D. W. Cope, G. Di Giovanni, S. J. Fyson, G. Orbán, A. C. Errington, M. L. Lorincz, T. M. Gould, D. A. Carter, V. Crunelli, Enhanced tonic $GABA_A$ inhibition in typical absence epilepsy. *Nat. Med.* **15**, 1392–1398 (2009).
17. A. N. Clarkson, B. S. Huang, S. E. Macisaac, I. Mody, S. T. Carmichael, Reducing excessive GABA-mediated tonic inhibition promotes functional recovery after stroke. *Nature* **468**, 305–309 (2010).
18. S. V. Dindot, B. A. Antalffy, M. B. Bhattacharjee, A. L. Beaudet, The Angelman syndrome ubiquitin ligase localizes to the synapse and nucleus, and maternal deficiency results in abnormal dendritic spine morphology. *Hum. Mol. Genet.* **17**, 111–118 (2008).
19. M. J. Wall, M. M. Usowicz, Development of action potential-dependent and independent spontaneous $GABA_A$ receptor-mediated currents in granule cells of postnatal rat cerebellum. *Eur. J. Neurosci.* **9**, 533–548 (1997).
20. D. J. Rossi, M. Hamann, Spillover-mediated transmission at inhibitory synapses promoted by high affinity $\alpha_6$ subunit $GABA_A$ receptors and glomerular geometry. *Neuron* **20**, 783–795 (1998).
21. V. Santhakumar, H. J. Hanchar, M. Wallner, R. W. Olsen, T. S. Otis, Contributions of the $GABA_A$ receptor α6 subunit to phasic and tonic inhibition revealed by a naturally occurring polymorphism in the α6 gene. *J. Neurosci.* **26**, 3357–3364 (2006).
22. A. Gadea, A. M. López-Colomé, Glial transporters for glutamate, glycine, and GABA: II. GABA transporters. *J. Neurosci. Res.* **63**, 461–468 (2001).
23. C. S. Chiu, S. Brickley, K. Jensen, A. Southwell, S. McKinney, S. Cull-Candy, I. Mody, H. A. Lester, GABA transporter deficiency causes tremor, ataxia, nervousness, and increased GABA-induced tonic conductance in cerebellum. *J. Neurosci.* **25**, 3234–3245 (2005).
24. R. M. Gustin, T. J. Bichell, M. Bubser, J. Daily, I. Filonova, D. Mrelashvili, A. Y. Deutch, R. J. Colbran, E. J. Weeber, K. F. Haas, Tissue-specific variation of Ube3a protein expression in rodents and in a mouse model of Angelman syndrome. *Neurobiol. Dis.* **39**, 283–291 (2010).
25. A. Togawa, T. Yamamoto, H. Suzuki, H. Fukasawa, N. Ohashi, Y. Fujigaki, K. Kitagawa, T. Hattori, M. Kitagawa, A. Hishida, Ubiquitin-dependent degradation of Smad2 is increased in the glomeruli of rats with anti-thymocyte serum nephritis. *Am. J. Pathol.* **163**, 1645–1652 (2003).
26. H. Fukasawa, T. Yamamoto, Y. Fujigaki, T. Misaki, N. Ohashi, T. Takayama, S. Suzuki, S. Mugiya, T. Oda, C. Uchida, K. Kitagawa, T. Hattori, H. Hayashi, S. Ozono, M. Kitagawa, A. Hishida,

Reduction of transforming growth factor-β type II receptor is caused by the enhanced ubiquitin-dependent degradation in human renal cell carcinoma. *Int. J. Cancer* **127**, 1517–1525 (2010).
27. V. M. Korkhov, H. Farhan, M. Freissmuth, H. H. Sitte, Oligomerization of the γ-aminobutyric acid transporter-1 is driven by an interplay of polar and hydrophobic interactions in transmembrane helix II. *J. Biol. Chem.* **279**, 55728–55736 (2004).
28. H. Farhan, V. Reiterer, V. M. Korkhov, J. A. Schmid, M. Freissmuth, H. H. Sitte, Concentrative export from the endoplasmic reticulum of the γ-aminobutyric acid transporter 1 requires binding to SEC24D. *J. Biol. Chem.* **282**, 7679–7689 (2007).
29. S. G. Brickley, S. G. Cull-Candy, M. Farrant, Development of a tonic form of synaptic inhibition in rat cerebellar granule cells resulting from persistent activation of $GABA_A$ receptors. *J. Physiol.* **497** (Pt. 3), 753–759 (1996).
30. M. Hamann, D. J. Rossi, D. Attwell, Tonic and spillover inhibition of granule cells control information flow through cerebellar cortex. *Neuron* **33**, 625–633 (2002).
31. P. Chadderton, T. W. Margrie, M. Häusser, Integration of quanta in cerebellar granule cells during sensory processing. *Nature* **428**, 856–860 (2004).
32. S. G. Brickley, V. Revilla, S. G. Cull-Candy, W. Wisden, M. Farrant, Adaptive regulation of neuronal excitability by a voltage-independent potassium conductance. *Nature* **409**, 88–92 (2001).
33. N. Brown, J. Kerby, T. P. Bonnert, P. J. Whiting, K. A. Wafford, Pharmacological characterization of a novel cell line expressing human $\alpha_4\beta_3\delta$ $GABA_A$ receptors. *Br. J. Pharmacol.* **136**, 965–974 (2002).
34. M. Womack, K. Khodakhah, Active contribution of dendrites to the tonic and trimodal patterns of activity in cerebellar Purkinje neurons. *J. Neurosci.* **22**, 10603–10612 (2002).
35. M. Sausbier, H. Hu, C. Arntz, S. Feil, S. Kamm, H. Adelsberger, U. Sausbier, C. A. Sailer, R. Feil, F. Hofmann, M. Korth, M. J. Shipston, H. G. Knaus, D. P. Wolfer, C. M. Pedroarena, J. F. Storm, P. Ruth, Cerebellar ataxia and Purkinje cell dysfunction caused by $Ca^{2+}$-activated $K^+$ channel deficiency. *Proc. Natl. Acad. Sci. U.S.A.* **101**, 9474–9478 (2004).
36. D. H. Heck, Y. Zhao, S. Roy, M. S. LeDoux, L. T. Reiter, Analysis of cerebellar function in *Ube3a*-deficient mice reveals novel genotype-specific behaviors. *Hum. Mol. Genet.* **17**, 2181–2189 (2008).
37. S. A. Mulherkar, N. R. Jana, Loss of dopaminergic neurons and resulting behavioural deficits in mouse model of Angelman syndrome. *Neurobiol. Dis.* **40**, 586–592 (2010).
38. E. M. Aloy, O. Weinmann, C. Pot, H. Kasper, D. A. Dodd, T. Rülicke, F. Rossi, M. E. Schwab, Synaptic destabilization by neuronal Nogo-A. *Brain Cell Biol.* **35**, 137–156 (2006).
39. T. Cremers, B. Ebert, Plasma and CNS concentrations of Gaboxadol in rats following subcutaneous administration. *Eur. J. Pharmacol.* **562**, 47–52 (2007).
40. M. Kaneda, M. Farrant, S. G. Cull-Candy, Whole-cell and single-channel currents activated by GABA and glycine in granule cells of the rat cerebellum. *J. Physiol.* **485** (Pt. 2), 419–435 (1995).
41. S. De Biasi, L. Vitellaro-Zuccarello, N. C. Brecha, Immunoreactivity for the GABA transporter-1 and GABA transporter-3 is restricted to astrocytes in the rat thalamus. A light and electron-microscopic immunolocalization. *Neuroscience* **83**, 815–828 (1998).
42. C. Kuenzle, M. Steinlin, G. Wohlrab, E. Boltshauser, B. Schmitt, Adverse effects of vigabatrin in Angelman syndrome. *Epilepsia* **39**, 1213–1215 (1998).
43. J. Voss, C. Sanchez, S. Michelsen, B. Ebert, Rotarod studies in the rat of the $GABA_A$ receptor agonist gaboxadol: Lack of ethanol potentiation and benzodiazepine cross-tolerance. *Eur. J. Pharmacol.* **482**, 215–222 (2003).
44. M. B. Herd, N. Foister, D. Chandra, D. R. Peden, G. E. Homanics, V. J. Brown, D. J. K. Balfour, J. J. Lambert, D. Belelli, Inhibition of thalamic excitability by 4,5,6,7-tetrahydroisoxazolo [4,5-c]pyridine-3-ol: A selective role for δ-$GABA_A$ receptors. *Eur. J. Neurosci.* **29**, 1177–1187 (2009).
45. P. D. Suzdak, C. Foged, K. E. Andersen, Quantitative autoradiographic characterization of the binding of [$^3$H]tiagabine (NNC 05-328) to the GABA uptake carrier. *Brain Res.* **647**, 231–241 (1994).
46. A. Friemel, B. Ebert, P. H. Hutson, P. Brust, K. Nieber, W. Deuther-Conrad, Postnatal development and kinetics of [$^3$H]gaboxadol binding in rat brain: In vitro homogenate binding and quantitative autoradiography. *Brain Res.* **1170**, 39–47 (2007).
47. H. Kaphzan, S. A. Buffington, J. I. Jung, M. N. Rasband, E. Klann, Alterations in intrinsic membrane properties and the axon initial segment in a mouse model of Angelman syndrome. *J. Neurosci.* **31**, 17637–17648 (2011).
48. I. van Welie, S. du Lac, Bidirectional control of BK channel open probability by CAMKII and PKC in medial vestibular nucleus neurons. *J. Neurophysiol.* **105**, 1651–1659 (2011).
49. G. Cheron, L. Servais, J. Wagstaff, B. Dan, Fast cerebellar oscillation associated with ataxia in a mouse model of Angelman syndrome. *Neuroscience* **130**, 631–637 (2005).
50. N. Asahina, T. Shiga, K. Egawa, H. Shiraishi, S. Kohsaka, S. Saitoh, [$^{11}$C]Flumazenil positron emission tomography analyses of brain gamma-aminobutyric acid type A receptors in Angelman syndrome. *J. Pediatr.* **152**, 546–549 (2008).
51. W. H. Roden, L. D. Peugh, L. A. Jansen, Altered $GABA_A$ receptor subunit expression and pharmacology in human Angelman syndrome cortex. *Neurosci. Lett.* **483**, 167–172 (2010).
52. F. Crestani, R. Keist, J. M. Fritschy, D. Benke, K. Vogt, L. Prut, H. Blüthmann, H. Möhler, U. Rudolph, Trace fear conditioning involves hippocampal $\alpha_5$ $GABA_A$ receptors. *Proc. Natl. Acad. Sci. U.S.A.* **99**, 8980–8985 (2002).
53. C. Altier, A. Garcia-Caballero, B. Simms, H. You, L. Chen, J. Walcher, H. W. Tedford, T. Hermosilla, G. W. Zamponi, The Cavβ subunit prevents RFP2-mediated ubiquitination and proteasomal degradation of L-type channels. *Nat. Neurosci.* **14**, 173–180 (2011).
54. A. K. Fu, K. W. Hung, W. Y. Fu, C. Shen, Y. Chen, J. Xia, K. O. Lai, N. Y. Ip, $APC^{Cdh1}$ mediates EphA4-dependent downregulation of AMPA receptors in homeostatic plasticity. *Nat. Neurosci.* **14**, 181–189 (2011).
55. C. Boehmer, G. Henke, R. Schniepp, M. Palmada, J. D. Rothstein, S. Bröer, F. Lang, Regulation of the glutamate transporter EAAT1 by the ubiquitin ligase Nedd4-2 and the serum and glucocorticoid-inducible kinase isoforms SGK1/3 and protein kinase B. *J. Neurochem.* **86**, 1181–1188 (2003).
56. C. Takayama, Y. Inoue, Developmental expression of GABA transporter-1 and 3 during formation of the GABAergic synapses in the mouse cerebellar cortex. *Brain Res. Dev. Brain Res.* **158**, 41–49 (2005).
57. M. Sato, M. P. Stryker, Genomic imprinting of experience-dependent cortical plasticity by the ubiquitin ligase gene *Ube3a*. *Proc. Natl. Acad. Sci. U.S.A.* **107**, 5611–5616 (2010).
58. P. I. Ortinski, J. R. Turner, A. Barberis, G. Motamedi, R. P. Yasuda, B. B. Wolfe, K. J. Kellar, S. Vicini, Deletion of the $GABA_A$ receptor α1 subunit increases tonic $GABA_A$ receptor current: A role for GABA uptake transporters. *J. Neurosci.* **26**, 9323–9331 (2006).
59. S. Mager, N. Kleinberger-Doron, G. I. Keshet, N. Davidson, B. I. Kanner, H. A. Lester, Ion binding and permeation at the GABA transporter GAT1. *J. Neurosci.* **16**, 5405–5414 (1996).
60. K. Kitagawa, Y. Hiramatsu, C. Uchida, T. Isobe, T. Hattori, T. Oda, K. Shibata, S. Nakamura, A. Kikuchi, M. Kitagawa, Fbw7 promotes ubiquitin-dependent degradation of c-Myb: Involvement of GSK3-mediated phosphorylation of Thr-572 in mouse c-Myb. *Oncogene* **28**, 2393–2405 (2009).
61. K. Inoue, S. Ueno, A. Fukuda, Interaction of neuron-specific $K^+$-$Cl^-$ cotransporter, KCC2, with brain-type creatine kinase. *FEBS Lett.* **564**, 131–135 (2004).
62. C. Uchida, S. Miwa, K. Kitagawa, T. Hattori, T. Isobe, S. Otani, T. Oda, H. Sugimura, T. Kamijo, K. Ookawa, H. Yasuda, M. Kitagawa, Enhanced Mdm2 activity inhibits pRB function via ubiquitin-dependent degradation. *EMBO J.* **24**, 160–169 (2005).
63. T. Sato, A modified method for lead staining of thin sections. *J. Electron Microsc.* **17**, 158–159 (1968).

**Acknowledgments:** We thank H. A. Lester (California Institute of Technology) and T. Ohta (St. Marianna University School of Medicine) for providing the pcDNA3.1-mGAT1 and pcDNA3-Myc3-E6AP (Ube3a) expression plasmids, respectively. **Funding:** This work was supported by a Grant-in-Aid for Young Scientists (B) from the Japan Society for the Promotion of Science #23791166 (K.E.); Grants-in-Aid for Scientific Research on Priority Areas from the Ministry of Education, Culture, Sports, Science, and Technology, Japan, #21026013 and 23115506 (to A.F.); and Grants-in-Aid for Scientific Research from the Japan Society for the Promotion of Science #22390041 (to A.F.). **Author contributions:** K.E., M.K., S.S., and A.F. participated in the design and interpretation of the data. K.E. performed the electrophysiological experiments. K.E. and M.T. performed the behavioral experiments. K.I., K.K., and M.K. performed the immunohistochemical experiments. C.T. performed electron microscopy. T.K. generated the Ube3a knockout mouse line. K.E. and A.F. wrote the manuscript. **Competing interests:** The authors declare that they have no competing interests.

Submitted 20 July 2012
Accepted 14 November 2012
Published 5 December 2012
10.1126/scitranslmed.3004655

**Citation:** K. Egawa, K. Kitagawa, K. Inoue, M. Takayama, C. Takayama, S. Saitoh, T. Kishino, M. Kitagawa, A. Fukuda, Decreased tonic inhibition in cerebellar granule cells causes motor dysfunction in a mouse model of Angelman syndrome. *Sci. Transl. Med.* **4**, 163ra157 (2012).

Cell. Mol. Life Sci.
DOI 10.1007/s00018-012-1232-x

Cellular and Molecular Life Sciences

REVIEW

# Roles of the Skp2/p27 axis in the progression of chronic nephropathy

**Sayuri Suzuki · Naro Ohashi · Masatoshi Kitagawa**

Received: 23 September 2012 / Revised: 14 November 2012 / Accepted: 3 December 2012


**Abstract** S-phase kinase-associated protein 2 (Skp2) is an F-box protein component of the Skp/Cullin/F-box-type E3 ubiquitin ligase that targets several cell cycle regulatory proteins for degradation through the ubiquitin-dependent pathway. Skp2-mediated degradation of p27, a cyclin-dependent kinase inhibitor, is involved in cell cycle regulation. Tubular epithelial cell proliferation is a characteristic feature of renal damage that is apparent in the early stages of nephropathy. The p27 level is associated with the progression of renal injury, and increased Skp2 expression in progressive nephropathy is implicated in decreases of p27 expression. In $Skp2^{-/-}$ mice, renal damage caused by unilateral ureteral obstruction (UUO) was ameliorated by p27 accumulation, mainly in tubular epithelial cells. However, the amelioration of UUO-induced renal injury in $Skp2^{-/-}$ mice was prevented by p27 deficiency in $Skp2^{-/-}/p27^{-/-}$ mice. These results suggest that the Skp2-mediated reduction in p27 is a pathogenic activity that occurs during the progression of nephropathy. Here, we discuss the roles of the Skp2/p27 axis and/or related signaling pathways/components in the progression of chronic nephropathy.

**Keywords** Ubiquitin-proteasome · Ubiquitin ligase · Chronic nephropathy · p27 · Skp2

S. Suzuki · M. Kitagawa (✉)
Department of Molecular Biology, Hamamatsu University School of Medicine, 1-20-1 Handayama, Hamamatsu 431-3192, Japan
e-mail: kitamasa@hama-med.ac.jp

N. Ohashi
Internal Medicine 1, Hamamatsu University School of Medicine, Hamamatsu, Japan

## Introduction

Cell proliferation is a fundamental biological mechanism that involves transit through the cell cycle. It is regulated by a network of proteins including cyclins, cyclin-dependent kinases (CDKs) [1], and CDK inhibitors (CKIs) [2]. The CKI $p27^{Kip1}$ (p27) is a negative regulator that halts progression from the G1 phase to the S phase in the cell cycle. p27 is abundantly expressed in most normal quiescent cells, whereas its level declines when cells are stimulated to proliferate in response to mitotic stimuli, allowing progression to the S phase [3, 4]. The ubiquitin-proteasome pathway for protein degradation plays an important role in regulating the abundance of cell cycle regulatory proteins [5, 6]. Protein degradation via the ubiquitin-proteasome pathway is rapid and substrate-specific, which is consistent with its role in controlling fluctuations in the intracellular concentrations of cyclins and CKIs. S-phase kinase-associated protein 2 (Skp2) is an F-box protein component of the Skp/Cullin/F-box (SCF)-type E3 ubiquitin ligase that plays important roles in regulating the progression to the S phase. p27 is phosphorylated at threonine residue 187 (Thr187) by CDK2/cyclin E. The SCF/Skp2 complex interacts with phosphorylated p27 to promote p27 degradation through the ubiquitin-proteasome pathway [7, 8]. The cdc kinase subunit 1 (Cks1) is an essential cofactor for SCF/Skp2 ubiquitin ligase to ubiquitylate p27. Cks1 recognizes and binds to Thr187-phosphorylated p27 and induces rigid binding between Skp2 and p27 [9, 10]. p27 is stabilized in Skp2-deficient mice [11]. Therefore, proteasomal ubiquitin-dependent degradation of p27 is specifically controlled by the SCF/Skp2/Cks1 complex.

In the kidney, cell proliferation is thought to represent a central response to renal injury culminating in end-stage renal disease caused by the progression of tubulointerstitial

Published online: 20 December 2012

fibrosis [ ]. Disruption of the balance between cell proliferation and apoptosis leads to unchecked apoptosis of damaged tubular epithelial cells resulting in progressive tubular cell loss, renal tubular atrophy, and advanced interstitial fibrosis [ ].

## Unilateral ureteral obstruction (UUO) and anti-thymocyte serum (ATS) are models of chronic nephropathy

UUO is a widely used model of kidney disease associated with progressive tubulointerstitial damage. This method has been used to identify many of the cellular and molecular events that occur during the progression of renal fibrosis, including events associated with cell proliferation and apoptosis [ –16]. UUO kidneys show elevated expression levels of monocyte chemoattractant protein-1 (MCP-1), vascular cell adhesion molecule-1 (VCAM-1), and intercellular adhesion molecule-1 (ICAM-1), which promote monocyte infiltration and kidney inflammation [ , ]. It is generally believed that renal tubule dilation occurs as a result of increased hydrostatic pressure following obstruction. However, it was also reported that decreases in renal blood flow and the glomerular filtration rate both promote macrophage invasion into the renal interstitium. The infiltrated macrophages release various cytokines, including TNF-α [ ]. The cytokine signals and hydrostatic pressure may act collaboratively to stimulate epithelial cell proliferation, which results in an increased number of tubular epithelial cells. We previously reported that tubule dilation is correlated with the increase in number of epithelial cells and enhanced tubular epithelial cell proliferation in the obstructed kidney [ ]. Taken together, these results suggest that hydrostatic pressure and tubular epithelial cell proliferation are involved

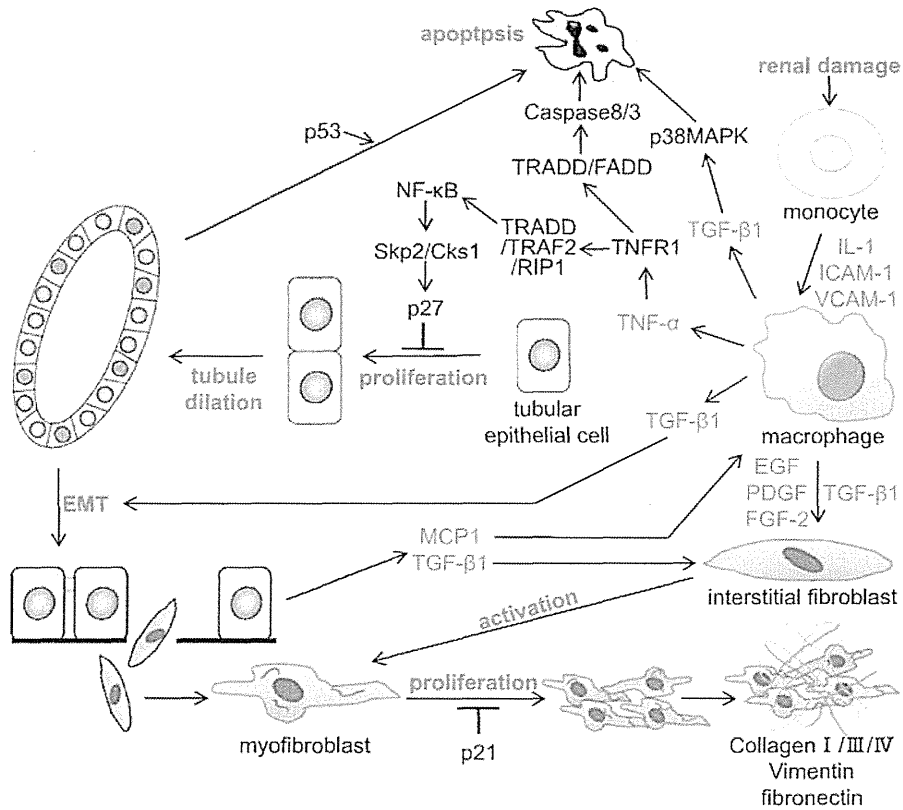


**Fig. 1** The signal transduction pathways involved in the progression of chronic nephropathy. Following renal damage, infiltrated macrophages in the tubulointerstitium release cytokines such as tumor necrosis factor-α (TNF-α) and transforming growth factor-β1 (TGF-β1). TNF-α binds to TNF receptor 1 (TNFR1) and forms a complex with TNFR-associated death domain (TRADD), TNF associated factor 2 (TRAF2), and receptor interaction protein 1 (RIP1). This complex activates nuclear factor (NF)-κB, which induces Skp2 and Cks1. Upregulation of Skp2/Cks1 promotes p27 degradation in tubular epithelial cells, allowing proliferation of tubular epithelial cells and tubule dilation following the increase of tubular epithelial cell number. The tubular epithelial cells undergo epithelial-mesenchymal transition (EMT) by stimulation of TGF-β1, and the resulting fibroblasts migrate to the tubulointerstitium. Cytokines including TGF-β1 activate fibroblasts; activated myofibroblasts produce extracellular matrix components, such as collagen, vimentin, and fibronectin. Meanwhile, TNF-α and TGF-β1 induce tubular epithelial cell apoptosis. *IL-1* interleukin-1, *ICAM-1* intercellular adhesion molecule-1, *VCAM-1* vascular cell adhesion molecule-1, *EGF* epidermal growth factor, *PDGF* platelet-derived growth factor, *FGF-2* fibroblast growth factor-2, *FADD* Fas-associated death domain protein, *MAPK* mitogen-activated protein kinase